

Long-term X-Ray Spectral Variability in AGN from the Palomar sample observed by *Swift*

S. D. Connolly^{1*}, I.M. McHardy¹, C. J. Skipper^{1,2}, D. Emmanoulopoulos¹

¹*Physics & Astronomy, University of Southampton, Highfield, Southampton, SO17 1BJ, UK*

²*Jodrell Bank Centre for Astrophysics, Alan Turing Building, The University of Manchester, Manchester, M13 9PL, UK*

2 May 2018

ABSTRACT

We present X-ray spectral variability of 24 local active galactic nuclei (AGN) from the Palomar sample of nearby galaxies, as observed mainly by *Swift*. From hardness ratio measurements, we find that 18 AGN with low accretion rates show hardening with increasing count rate, converse to the softer-when-brighter behaviour normally observed in AGN with higher accretion rates. Two AGN show softening with increasing count rate, two show more complex behaviour, and two do not show any simple relationship.

Sufficient data were available for the spectra of 13 AGN to be summed in flux-bins. In 9 of these sources, correlated luminosity-dependent changes in the photon index (Γ) of a power-law component are found to be the main cause of hardness variability. For 6 objects, with a low accretion rate as a fraction of the Eddington rate (\dot{m}_{Edd}), Γ is anticorrelated with \dot{m}_{Edd} , i.e. ‘harder-when-brighter’ behaviour is observed. The 3 higher- \dot{m}_{Edd} -rate objects show a positive correlation between Γ and \dot{m}_{Edd} . This transition from harder-when-brighter at low \dot{m}_{Edd} to softer-when-brighter at high \dot{m}_{Edd} can be explained by a change in the dominant source of seed-photons for X-ray emission from cyclo-synchrotron emission from the Comptonising corona itself to thermal seed-photons from the accretion disc. This transition is also seen in the ‘hard state’ of black hole X-ray binaries (BHXRBs). The results support the idea that LINERs are analogues of BHXRBs in the hard state and that Seyferts are analogues of BHXRBs in either the high-accretion-rate end of the hard state or in the hard-intermediate state.

Key words: X-rays: galaxies galaxies: active galaxies: nuclei - galaxies: individual:M81

1 INTRODUCTION

In many studies of black holes with relatively high accretion rates as a fraction of their Eddington accretion rates (\dot{m}_{Edd}), including both single-epoch observations of samples of objects and multi-epoch observations of individual objects, the X-ray spectrum becomes softer as the luminosity increases. This softer-when-brighter behaviour is seen in both black hole X-ray binary systems (BHXRBs) (e.g. Gu & Cao 2009) and in AGN (e.g. McHardy et al. 1998; Sobolewska & Papadakis 2009; Shemmer et al. 2006). This behaviour is usually attributed to a real increase in the photon index, Γ , of the power law assumed to describe the shape of the intrinsic emission spectrum.

This ‘softer-when-brighter’ correlation has not been found to hold, however, for lower accretion rate systems. In a sample of single-epoch observations of low-luminosity AGN (LLAGN), Gu & Cao (2009) found Γ to be *anticorrelated* with the accretion rate (i.e. ‘harder-when-brighter’). A similar conclusion was reached by both Younes et al. (2011) and Hernández-García et al. (2014) in samples of low-ionisation nuclear emission region galaxies (LINERs). Harder-when-brighter behaviour has also been observed in multi-epoch observations of individual BHXRBs by e.g. Kalemci et al. (2004) and Yuan et al. (2007). This behaviour has, however, only been seen once in multi-epoch observations of in an individual AGN, the LLAGN NGC 7213, by Emmanoulopoulos et al. (2012), and was once again thought to be caused by an anticorrelation between Γ and the accretion rate.

* E-mail: sdc1g08@soton.ac.uk

In a study of a sample of BXRBs by Wu & Gu (2008), harder-when-brighter behaviour was observed below a ‘critical’ accretion rate (\dot{m}_{crit}) of $\sim 0.01 \dot{m}_{\text{Edd}}$, above which softer-when-brighter behaviour was seen. The same change in behaviour above a certain critical accretion rate has also been seen into multi-epoch observations of the XRB Cyg X-1 (Skipper et al. 2013; Axelsson et al. 2008). Single-epoch observations of large samples of AGN have shown that they follow the same behaviour globally (Constantin et al. 2009; Gu & Cao 2009; Younes et al. 2011), supporting the idea that AGN behave in a similar way to BXRBs. Note that the change from harder-when-brighter to softer-when-brighter at \dot{m}_{crit} occurs within the hard state and is not considered to be a state transition. The accretion rate below which BXRBs are never seen in the soft state ($\sim 2\% \dot{m}_{\text{Edd}}$; Maccarone et al. (2003)) occurs factors of 2-3 above \dot{m}_{crit} .

At extremely low accretion rate ($< \sim 10^{-6} \dot{m}_{\text{Edd}}$), the behaviour has been found to change once again, with the spectral hardness no longer changing, which is thought to be due to Γ saturating at a relatively constant, and high, level as the accretion rate decreases (Yang et al. 2015). This saturation is once again seen in observations of both AGN and BXRBs, using a small number of observations from large samples of sources (Yang et al. 2015; Gu & Cao 2009; Hernández-García et al. 2013).

Due to a number of similarities, including a low accretion rate and radio loudness, it has been suggested that LLAGN are the analogues of the ‘hard state’ of BXRBs, whilst more luminous Seyferts and quasars are the analogues of ‘soft-state’ BXRBs. In this paper we will re-examine these analogies.

The change in the relationship between the Γ and \dot{m}_{Edd} in these systems at a particular critical \dot{m}_{Edd} from a negative correlation to a positive correlation as \dot{m}_{Edd} increases implies that the seed photon source to the X-ray corona is changing (e.g. Emmanoulopoulos et al. 2012; Skipper et al. 2013). It has been suggested that the reason for this change may be that the accretion disc is transitioning from an advection dominated accretion flow (ADAF) to a standard thin disc as \dot{m}_{Edd} increases (Esin et al. 1997; Narayan 1994; Wu & Gu 2008; Constantin et al. 2009). In ADAF models, an increase in \dot{m}_{Edd} leads to an increasing optical depth and hence to a higher Compton parameter in the hot accretion flow, ‘hardening’ the X-ray spectrum and producing an anticorrelation between Γ and \dot{m}_{Edd} , and therefore harder-when-brighter behaviour.

The ‘hard state’, with which ADAFs are associated in BXRBs, is usually also associated with the presence of a jet (Russell et al. 2010). The X-ray emission mechanism in BXRBs is not known unambiguously, but self-Comptonisation of synchrotron emission from the corona, or possibly from a jet at higher energies, is a possibility. Synchrotron self-Compton emission dominates blazar jet emission, with luminosity-increases associated with an injection of hard-spectrum electrons, e.g. from a shock (e.g. Ghisellini et al. 2009). The harder-when-brighter spectral relationship is commonly observed in blazars for this reason (e.g. Krawczynski et al. 2004; Gliozzi et al. 2006; Zhang et al. 2006) and could therefore also explain the same behaviour in LLAGN (Emmanoulopoulos et al. 2012).

In an ADAF, the inner edge of the optically thick part

of the disc is truncated a long way from the black hole. Further possible explanations for harder-when-brighter behaviour which do not require a truncated disc also exist, for example by invoking a outflowing hot thermal corona - for details see Sobolewska et al. (2011) and references therein.

In this study we present results on changes in hardness with luminosity of a sample of 24 AGN from the Palomar sample (Ho et al. 1997a) which have been observed by *Swift*. For those sources for which there is enough data, spectral fitting is performed with a variety of models, and changes in Γ with luminosity are measured.

The objects cover a range of masses between $5 \times 10^4 M_{\odot}$ and $8 \times 10^9 M_{\odot}$ and a range of \dot{m}_{Edd} between 10^{-6} and 0.5 (see Table 11). Approximately half of these objects possess accretion rates which lie in the regime in which softer-when-brighter behaviour is expected ($\dot{m}_{\text{Edd}} \geq 10^{-3}$). The rest occupy the accretion rate range ($\dot{m}_{\text{Edd}} \sim 10^{-6} - 10^{-3}$) in which individual XRBs (e.g. Axelsson et al. 2008; Skipper et al. 2013) and samples of AGN show harder-when-brighter behaviour. We also include NGC 7213 in our discussion, using the data from Emmanoulopoulos et al. (2012).

2 OBSERVATIONS & DATA REDUCTION

2.1 The AGN Sample

The sample used in this study consists of all known AGN in the Palomar sample of galaxies for which there is sufficient data for meaningful analysis. The Palomar sample contains 163 such objects (Seyfert galaxies and LINERs), 70 of which have been observed by *Swift*. So that sufficient data exist for at least a rudimentary spectral analysis, only objects for which there are a total of > 350 total photon counts and 4 or more separate observations were included in the analysis, leaving a final sample of 24 AGN. Table 1 gives a summary of the *Swift* observations of each of the selected AGN. The Palomar sample contains almost every galaxy in the northern sky with a magnitude of $B_T > 12.5$; the AGN within this sample are therefore all relatively nearby and a large fraction of them are low-luminosity - 85% lie below $L(\text{H}\alpha) = 10^{40} \text{ergs s}^{-1}$ (Ho et al. 1997a,b). As our sample contains only a relatively small subset of the Palomar AGN sample it is not statistically complete. However, whilst some galaxies were observed because they contained known AGN, others were observed for different reasons, e.g. because they contained a supernova, thus the subset is not particularly biased.

The data for all Palomar AGN except NGC 3998 were obtained by *Swift* and, in almost all cases, are composed of observations from a number of different programmes covering a number of years. The data for NGC 3998 are from a single campaign by the *Rossi X-ray Timing Explorer (RXTE)*, a preliminary analysis of which is described in Skipper (2013); whilst there are some *Swift* data available for NGC 3998, the *RXTE* data are of better quality.

In all *Swift* pointings, the observations were performed using the *Swift* XRT in ‘photon counting mode’. Exposure times of individual good time interval (GTI) observations ranged from less than 10 seconds to over 10^4 seconds. In each case, GTIs were excluded if they had a low signal-to-noise

Object	Observations	GTIs	Start & end date	Total exposure (s)	Total counts	No. summed spectra
NGC 315	5	42	2007-05-31 - 2009-03-03	26054	644	1
NGC 1052	21	126	2007-01-19 - 2011-03-06	81041	3043	3
NGC 1068 (M77)	13	44	2007-06-19 - 2015-02-05	32681	15819	5
NGC 2655	33	120	2011-01-11 - 2014-12-31	60351	1056	1
NGC 3031 (M81)	605	1033	2005-04-21 - 2014-06-22	771530	205159	28
NGC 3147	28	63	2009-01-11 - 2014-07-13	52929	2417	3
NGC 3226	26	63	2008-10-28 - 2015-07-06	52841	699	1
NGC 3227	26	63	2008-10-28 - 2015-05-23	19269	38816	10
NGC 3628	6	32	2006-11-12 - 2014-07-21	26518	379	1
NGC 3998	2	20	2007-04-20 - 2007-04-29	27285	6362	4
NGC 3998 [†]	376	376	2010-12-31 - 2011-12-26	287568	7628314	25
NGC 4051	55	100	2009-02-14 - 2013-10-10	58002	30821	10
NGC 4151	5	33	2005-12-26 - 2012-11-12	27387	17808	7
NGC 4258 (M106)	12	8	2008-03-01 - 2014-06-22	32238	1270	1
NGC 4321 (M100)	26	88	2005-11-06 - 2011-04-15	27426	282	1
NGC 4388	4	34	2005-12-27 - 2008-05-09	10594	1219	4
NGC 4395	225	412	2005-12-31 - 2013-05-10	302125	34277	22
NGC 4486 (M87)	19	46	2006-12-23 - 2015-05-18	29601	4264	4
NGC 4472 (M49)	6	19	2007-11-13 - 2010-03-30	14298	1268	1
NGC 4579 (M58)	27	41	2007-05-15 - 2007-05-18	20463	3555	3
NGC 4736 (M94)	18	39	2013-04-15 - 2015-05-12	23700	104	1
NGC 5194 (M51)	112	261	2005-06-30 - 2014-09-24	233095	5599	1
NGC 5548	656	878	2005-04-08 - 2014-06-21	574670	206387	42
NGC 5806	49	147	2012-01-14 - 2014-09-17	141994	381	1
NGC 7331	34	90	2007-02-12 - 2015-05-19	77403	616	1

Table 1. Details of the observations of the 24 AGN considered in this study. All data are from *Swift* except for the observations of NGC 3998 denoted by [†], from *RXTE*. The number of summed spectra is also given, denoting the number of flux bins into which the observations for each source were divided. Where the number is one, all the observations for that source were summed into a single spectrum (i.e. not flux-binned).

ratio ($S/N < 3$), very short exposure time ($T_{\text{exp}} < 50$ s) or the source was in close proximity to bad pixels. The raw data for all *Swift* XRT observations were downloaded from the HEASARC archive¹.

In addition to the data from this work, we also include data from NGC 7213 (Emmanoulopoulos et al. 2012) in the discussion, to allow comparison with what was, until now, the only confirmed detection of harder-when-brighter behaviour in an individual AGN. NGC 7213 is not part of the Palomar sample, and has not been observed extensively by *Swift*. However, it has been observed extensively (882 times) by *RXTE* and is known to possess a relatively simple power law spectrum (Emmanoulopoulos et al. 2013). We therefore do not include NGC 7213 within our discussion of *Swift* spectral fitting (Section 5) or of the properties of the Palomar sample, but take the results of the *RXTE* spectral fitting from Emmanoulopoulos et al. (2012).

2.2 Data Reduction

The XRT data were reduced using our automatic pipeline, described in e.g. Cameron et al. (2012), Connolly et al. (2014). The most recent version of the standard *Swift* XRT-PIPELINE software (versions 0.12.4 - 0.12.6) was used in each case. Spectra and light curves were extracted using the XSELECT tool, using flux-dependent source and background extraction regions chosen such that background contamination at faint fluxes was minimised, and to account

for the effects of pile-up at high fluxes. The effects of vignetting and the presence of bad pixels and columns on the CCD were removed by using the *Swift* XRTEXPOMAP and XRTMKARF tools to create an exposure map and an ancillary response file (ARF) for each visit. The relevant redistribution matrix file (RMF) from the *Swift* calibration database was also used in each case. The local X-ray background was estimated and subtracted from the instrumental count rates, using the area-scaled count rate measured in a background annulus region. The observed XRT count rates were corrected to take into account the fraction of counts lost due to bad pixels and columns, vignetting effects, and the finite extraction aperture (including regions excised in order to mitigate pileup effects).

RXTE observed NGC 3998 376 times under our own proposal 96398, from 2010 Dec 31 until 2011 Dec 26, and with exposure times of between 542 seconds and 6,770 seconds. The earlier observations were each separated by a period of roughly two days, but after approximately 2011 Oct 25 the frequency of observations increased to roughly once every six hours. All the data reduction was performed only upon the standard-2 data, with a time-resolution of 16 s.

For each observation a GTI was generated based upon the spacecraft elevation angle being greater than 10 degrees, the pointing offset being less than 0.02 degrees, and the time since the last south Atlantic anomaly (SAA) being at least 30 minutes. Synthetic background data were generated using the script RUNPCABACKEST with the faint background model (pca_bkgd_cmfaint17_eMv20051128.mdl), and suitable response files were created using PCARSP.

¹ <http://heasarc.gsfc.nasa.gov/cgi-bin/W3Browse/swift.pl>

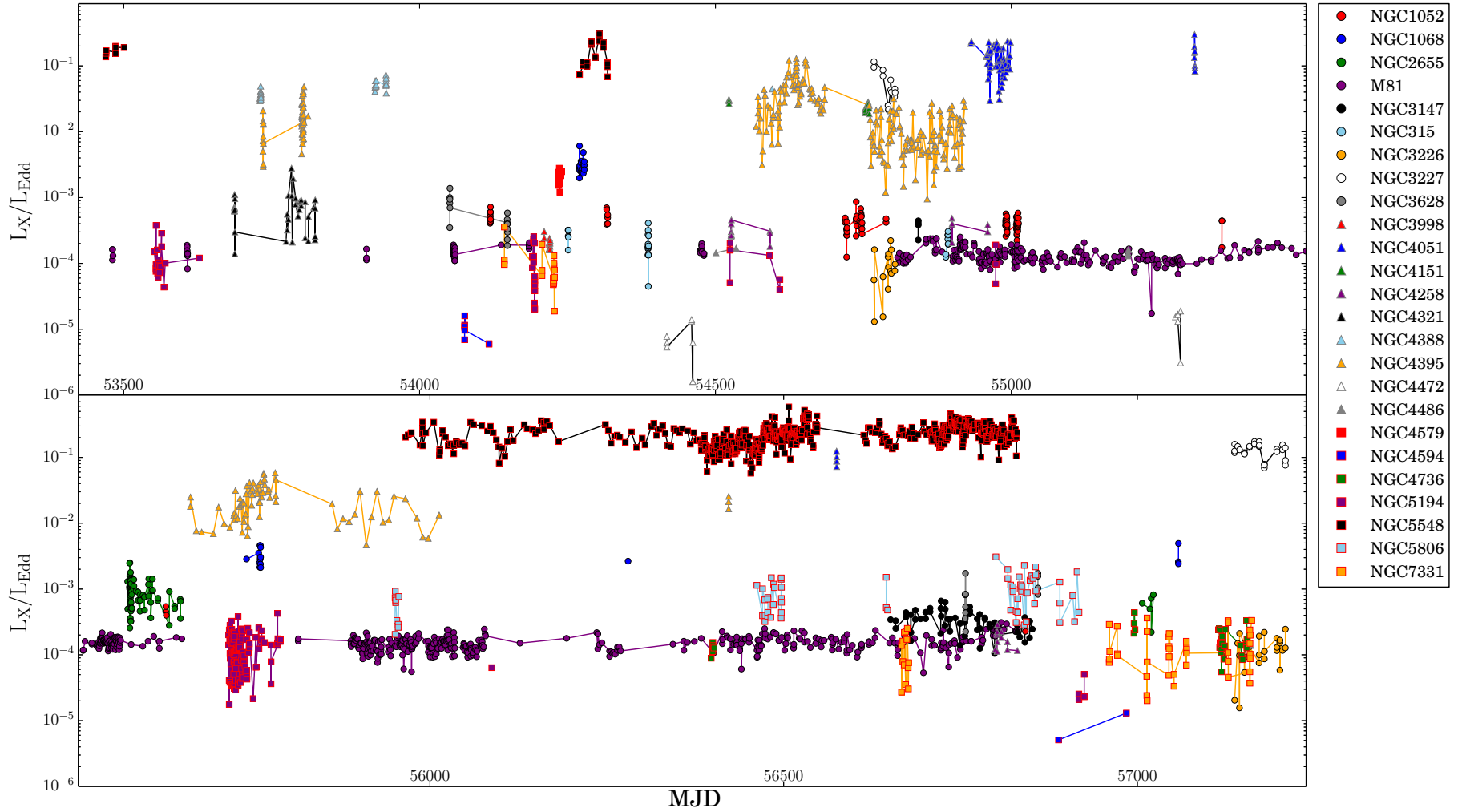


Figure 1. Light curve showing the ratio of the X-ray Luminosity to the Eddington Luminosity of each of the sources over time, showing the large range of Eddington rates present in the sample. The light curve is split into two sections for clarity.

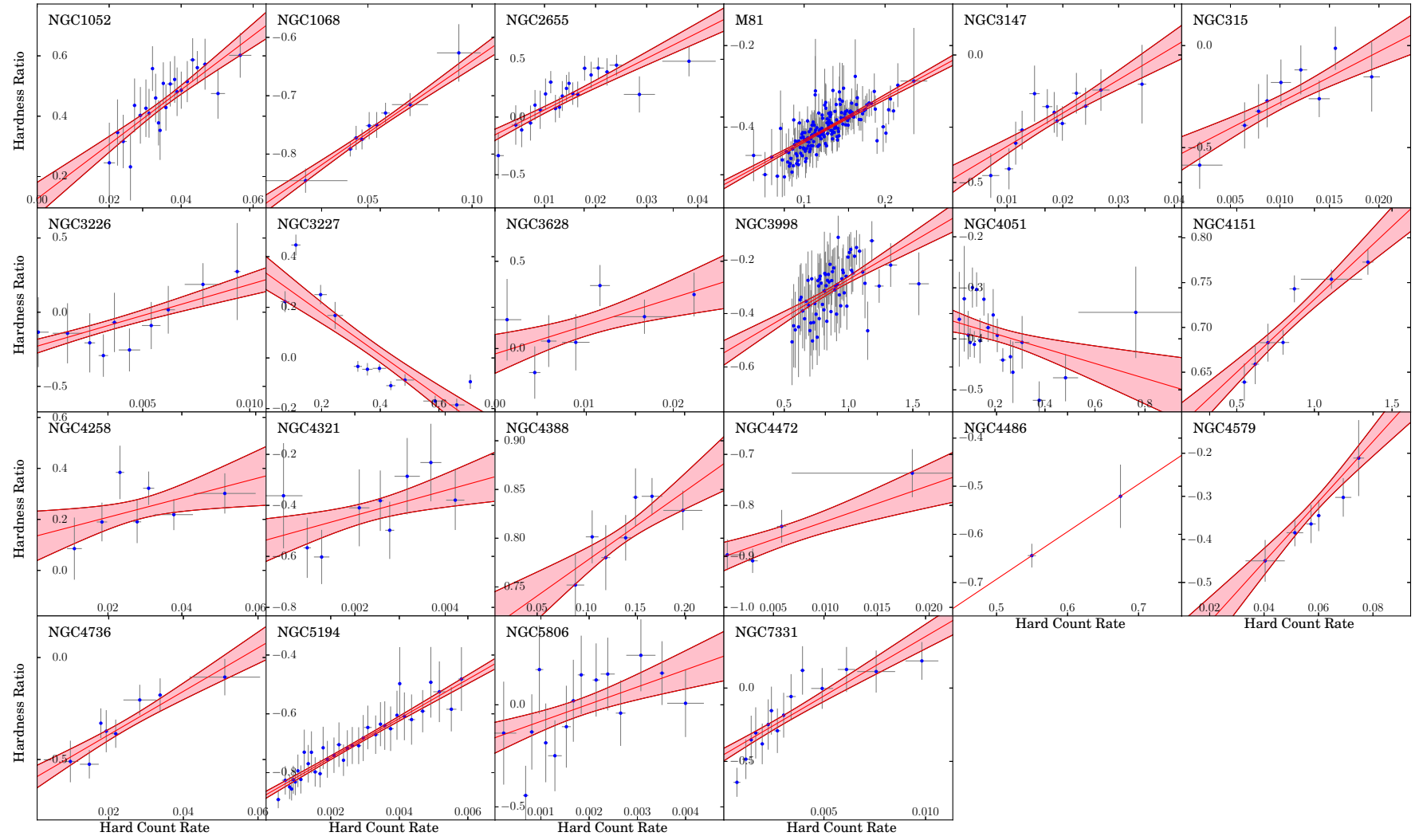


Figure 2. The hardness ratio of the spectrum of each *Swift* object using the 0.5-2 and 2-10 keV bands, plotted against its 2-10 keV count rate, and the hardness ratio of NGC 3998 using the 3.3-7 and 7-20 keV bands, plotted against its 7-20 keV count rate. The data are binned into bins of 10 data points. Error bars show the one-sigma confidence levels. In each case, the red line shows the best-fitting linear model and the pink region bounded by red indicates the one-sigma error region of the model parameters. A clear correlation between the two parameters, either positive or negative, is present in all objects except NGC 4321 and NGC 4486. NGC 4486 possessed too little data for meaningful binning with more than ten bins, so errors are not given.

Spectra were extracted from the standard-2 data and the background data for all layers of PCU 2 using SAEXTRACT, and subsequently rebinned using RBNPHA into 14 channels. All the analysis described in this paper uses channels 2-13, which roughly corresponds to the energy range 3.3 to 20 keV. The observations covered a large range of exposure times, with many being too short for useful spectral analysis. In many cases, time-binning would not have produced spectra of sufficient quality for meaningful spectral analysis without using broad time bins, which would itself have lead to spectra consisting of data taken across a large range of fluxes. Whilst there is some scatter in the hardness of a given source at a given flux, the scatter is not large (see Section 3), indicating that spectral shape is a function mainly of luminosity rather than of time. Thus, flux-binning is legitimate. To improve the S/N, the data were therefore binned in flux.

Where there were sufficient data, the *Swift* spectra were binned such that each resultant summed spectrum had a minimum of 1000 total counts and a maximum width in count rate of 5×10^{-3} counts s^{-1} , with the exception of NGC 1052, NGC 3147 and NGC4579 which, due to fewer data, were binned with a minimum of 900, 600 and 900 total counts per spectrum, respectively. For objects for which there were insufficient data to obtain at least 3 flux-binned spectra with a minimum of 350 total counts, a total summed spectrum was produced. The *RXTE* spectra, having a considerably higher count rate but lower signal-to-noise ratio, were binned such that each resultant summed spectrum had a minimum of 8000 total counts per spectrum. The number of summed spectra produced for each source is shown in Table 1.

The spectra were combined using the *HEADAS* tool ‘addspec’. As the amount of data varied between sources, the number of spectra produced in each case also varied. The energy channels of each of the summed spectra were then grouped, using the *HEADAS* tool ‘grppha’, such that each group contained a minimum of 15 counts.

The light curves of the ratio of the X-ray luminosity to the Eddington luminosity of each of the 24 AGN are shown in Fig. 1.

3 SPECTRAL HARDNESS

For the objects observed by *Swift*, hard emission is defined as 2.0 – 10.0 keV and soft emission as 0.5 – 2.0 keV; for NGC 3998 (observed by *RXTE*), hard emission is defined as 7.0 – 20.0 keV and soft emission as 3.3 – 7.0 keV. In all cases, the hardness ratio is defined as:

$$\text{Hardness Ratio} = \frac{H - S}{H + S} \quad (1)$$

where ‘H’ is the hard count rate and (‘S’) is the soft count rate. Plots of the hardness ratio against the hard count rate of each object are shown in Figs. 3 and 2. These plots show, in a model-independent way, the way in which the spectrum of a given source is changing with increasing luminosity; if the spectral hardness increases with increasing luminosity, the source is harder-when-brighter, if the opposite is true the source is softer-when-brighter. For 22 of the 24 AGN, the hardness ratio changed with luminosity in an

approximately linear way. The hardness ratios vs. luminosity of these objects were fitted with a linear model in order to determine numerically whether they were harder- or softer-when-brighter. In each case, errors on the best-fitting parameters of the linear fits were calculated using 10000 Monte Carlo simulations in which the data were varied within their error distributions (assuming Gaussian errors) and refitted. The reduced χ^2 ($\chi_R^2 = \chi^2/DoF$) and best-fitting parameters from these fits are shown in Table 2; the best-fitting lines and the errors on the parameters of the lines are also shown in the hardness ratio vs. luminosity plots in Fig. 2.

NGC 4395 and NGC 5548 showed more complex variations in hardness ratio with increasing luminosity and were not well fit by a linear model. Both objects show evidence of being very soft at low luminosity and hardening rapidly with increasing luminosity, then changing to becoming softer-when-brighter at higher luminosity (see Fig. 3). This behaviour is also very similar to that observed in the Seyfert galaxies NGC 1365 and Mkn 335 (Connolly et al. 2014; Connolly 2015).

The linear fits to the hardness ratio vs. count rate data showed that 18 of the AGN possess harder-when-brighter behaviour. In addition to NGC 4395 and NGC 5548, two other sources showed softer-when-brighter behaviour. Two of the sources (NGC 4486 and NGC 4321) could not be constrained as being either harder- or softer-when-brighter, as errors in the gradients of the linear fits to their hardness ratio vs. count rate data do not constrain the gradients to be positive or negative. A high fraction (72%) of the sample therefore show harder-when-brighter behaviour.

4 RESOLVING A CONSTANT SPECTRAL COMPONENT

Whilst the hardness ratio vs. flux plots indicate that there is a division in the behaviour of spectral variation in the AGN sample, the causes of the spectral variation cannot be discerned from hardness ratio changes alone. If the spectrum is a simple absorbed power law, with no or constant absorption, correlated hardness changes imply changes in the photon index which are correlated with luminosity. However, a hardness ratio correlated with luminosity would also be seen if an additional constant soft component is present in the spectrum, or could be produced by variable absorption. In both of these cases, the photon index of the underlying power law would not be required to vary.

A constant soft spectral component can be produced by background contamination from hot gas due to circumnuclear star formation, which is seen in some AGN spectra (Nemmen et al. 2006; Wang et al. 2009; Perez-Olea & Colina 1996). As the source brightens, the contribution of such a component would become smaller, increasing the hardness of the overall spectrum without the need for any change in the photon index. This soft component must, however, be luminous enough to produce the observed hardness changes.

A model-independent method to determine whether a constant spectral component is present, and if so what form it takes, is to plot the flux in different X-ray bands against one another (see e.g. Taylor et al. 2003). If one assumes a linear relationship between two bands, a linear model can

Object	χ^2/DoF	Gradient	Intercept	Behaviour when brighter
NGC 315	0.70	$26.26^{+11.76}_{-9.39}$	$-0.53^{+0.11}_{-0.11}$	harder
NGC 1052	0.54	$8.95^{+2.33}_{-1.90}$	$0.14^{+0.07}_{-0.10}$	harder
NGC 1068	0.40	$2.44^{+0.96}_{-0.56}$	$-0.88^{+0.03}_{-0.06}$	harder
NGC 2655	1.04	$21.82^{+4.45}_{-4.67}$	$-0.15^{+0.07}_{-0.07}$	harder
NGC 3031	0.80	$1.10^{+0.13}_{-0.10}$	$-0.54^{+0.01}_{-0.01}$	harder
NGC 3147	0.54	$13.11^{+3.56}_{-3.21}$	$-0.49^{+0.07}_{-0.06}$	harder
NGC 3226	0.49	$40.52^{+17.39}_{-14.40}$	$-0.24^{+0.08}_{-0.07}$	harder
NGC 3227	13.44	$-0.83^{+0.06}_{-0.05}$	$0.34^{+0.03}_{-0.03}$	softer
NGC 3628	1.11	$14.32^{+9.07}_{-7.97}$	$-0.01^{+0.13}_{-0.14}$	harder
NGC 3998 [†]	2.43	$1.74^{+1.50}_{-0.67}$	$-0.53^{+0.07}_{-0.11}$	harder
NGC 4051	2.22	$-0.19^{+0.16}_{-0.18}$	$-0.34^{+0.04}_{-0.05}$	softer
NGC 4151	1.64	$0.16^{+0.03}_{-0.03}$	$0.57^{+0.02}_{-0.02}$	harder
NGC 4258	1.13	$3.69^{+3.70}_{-2.67}$	$0.12^{+0.11}_{-0.10}$	harder
NGC 4321	2.69	$25.69^{+30.60}_{-25.80}$	$-0.46^{+0.05}_{-0.05}$	undetermined
NGC 4388	0.76	$0.73^{+0.27}_{-0.27}$	$0.71^{+0.03}_{-0.04}$	harder
NGC 4395	14.27	$-1.75^{+0.18}_{-0.17}$	$0.40^{+0.02}_{-0.02}$	softer
NGC 4472	1.78	$7.81^{+7.95}_{-5.17}$	$-0.91^{+0.05}_{-0.05}$	harder
NGC 4486	0.68	0.04	-0.68	undetermined
NGC 4579	0.19	$6.38^{+3.12}_{-2.05}$	$-0.71^{+0.12}_{-0.18}$	harder
NGC 4736	0.80	$10.39^{+4.99}_{-2.88}$	$-0.57^{+0.08}_{-0.11}$	harder
NGC 5194	1.28	$35.59^{+11.66}_{-9.96}$	$-0.80^{+0.04}_{-0.03}$	harder
NGC 5548	5.03	$-0.32^{+0.03}_{-0.02}$	$0.32^{+0.01}_{-0.01}$	softer
NGC 5806	0.58	$105.89^{+25.23}_{-30.11}$	$-0.22^{+0.06}_{-0.04}$	harder
NGC 7331	0.86	$80.45^{+15.10}_{-15.01}$	$-0.46^{+0.06}_{-0.06}$	harder

Table 2. The reduced χ^2 and best-fit parameters (with one-sigma errors) for linear fits to the hardness ratio vs. 2 – 10keV count rate plots of each object (see Fig. 2). The behaviour of each source with increasing count rate is always shown, determined by whether the slope of the linear fit is positive (softer-when-brighter) or negative (harder-when-brighter). The behaviour of objects with increasing luminosity is ‘undetermined’ if the errors on the gradient of the fit cross zero. NGC 4486 possessed too little data for meaningful binning with more than ten bins, so errors are not given.

be fitted to the data and extrapolated to estimate the flux in one band when the other is at zero flux (see Fig. 4). If it is assumed that any constant component present becomes negligibly small at high energies, as is reasonable for models of e.g. emission from hot plasma due to star formation, a high-energy reference band can be used to find the flux of the lower-energy bands when the variable component is zero. In this way, the shape of the underlying constant spectral component can be estimated. If the spectral shape of any constant component is known, it is then possible to determine in a model-independent way whether this component is the sole cause of hardness changes with luminosity, or whether intrinsic variations in the spectrum are required.

The only harder-when-brighter source for which this method could produce reasonably well-constrained results was M81. The X-ray count rates in 7 soft energy bands (0.3-0.5, 0.5-1.0, 1.0-1.5, 1.5-2.0, 2-3, 3-4 and 4-5 keV) were plotted against the 5-10 keV hard energy band. These data were then fitted with a linear model in the same manner as were the hardness ratio vs. flux plots in Section 3. By assuming that there is no underlying component in the 5-10 keV band, the intercepts of these linear fits can be taken as the count rates of any soft component in each band. The bands all showed a weak positive correlation, with an average Pearson correlation coefficient of 0.32. Fig. 4 shows an example of a plot of the count rate in two bands in the spectrum of M81, the best-fitting linear model and the errors in its parameters.

The constant spectral component is measured in count space from the instrumental data and must therefore be de-

convolved using the instrumental response for *Swift* in the same way as for any other X-ray spectrum. A typical instrumental response matrix for *Swift* was therefore applied to the derived constant spectrum during spectral modelling. A significant excess was only found in 3 of the 7 bands, two of these were in the 0.5 – 1.5 keV range; Fig. 5 shows the extrapolated count rate in each band.

This spectrum was fitted with three models - a power law, a hot gas model (mekal) and combination of the two. None of the models fitted the spectrum well (χ^2_{R} of 3.31, 3.67 and 4.04, for 6, 6 and 4 degrees of freedom, respectively), however the power law was the best-fitting model. Whilst this model may not be a perfect physical approximation of the constant component, it may still be used to test the possibility that such a component is causing the observed spectral variability. The lack of a good spectral fit, combined with the lack of a significant excess rate in 4 of the 7 bands may indicate that a constant component is not present at all, or extremely weak; despite this, the model fitted to the extrapolated spectrum was used in subsequent spectral modelling of M81 in order to test whether its contribution would be large enough to cause the observed hardness changes, under the assumption that it may be real.

5 SPECTRAL MODELLING

Enough data existed for spectral fitting of 14 of the 24 AGN at multiple flux levels. A set of models, in increasing degrees of complexity from a simple power law to a partially cov-

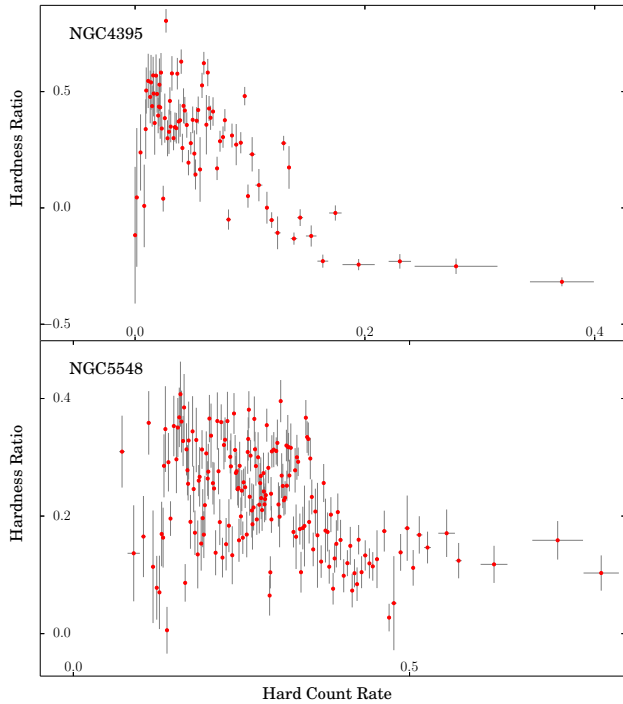


Figure 3. The hardness ratio of the spectra of NGC 4395 and NGC 5548 using the 0.5-2 and 2-10 keV bands, plotted against the 2-10 keV count rate. The data are binned into bins of 10 data points. Error bars show the one-sigma confidence levels. Both objects show more complex behaviour in their hardness ratios with increasing count rate when compared to the other objects. Both also show a general softer-when-brighter trend at intermediate count rates.

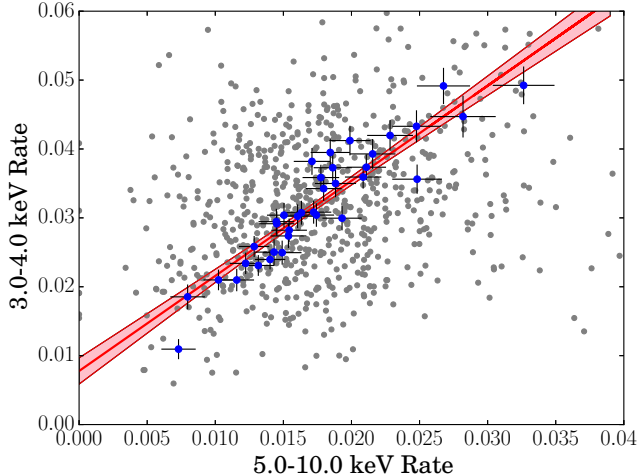


Figure 4. An example of a flux-flux diagram for M81, of the 3-4 v. 5-10 keV bands (binned). Blue points are binned data, with a minimum of 20 points per bin. Grey points shown behind are unbinned data. Error bars show the one-sigma confidence levels. The red line shows the best-fitting model, assuming a linear trend, and the pink region bounded by red indicates the one-sigma error region of the model parameters.

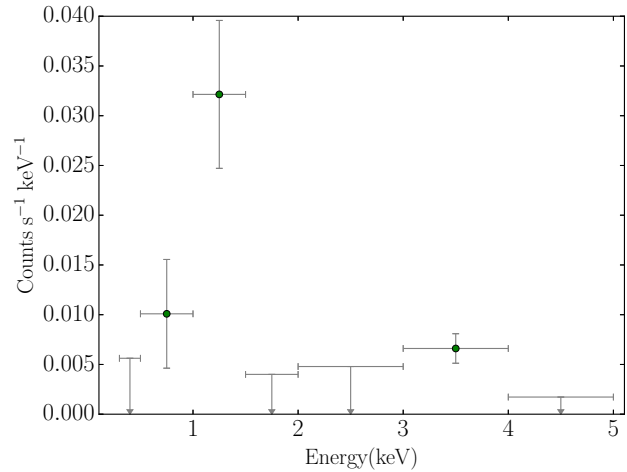


Figure 5. The constant, soft component of the spectrum of M81, assuming a linear relationship between the flux in different bands and zero flux in the 5-10 keV band. The data are folded through a typical response for *Swift*.

ered power law (see Table 3), were successively fitted to the spectra of each source until a good fit was found, using the XSPEC 12.7 analysis package (Arnaud 1996). Models were fitted to data in the 0.5 – 10keV energy range in all cases except that of the NGC 3998 *RXTE* data, for which the 3 – 20keV energy range was used. In all models, a neutral absorber whose column was fixed at the Galactic column in the direction of the source was included.

Table 3 contains descriptions of all of the spectral models fitted to the spectra. In all cases, the model was fitted simultaneously to all of the flux-binned spectra for a given object - for some models, some parameters were ‘tied’, meaning they were allow to vary, but constrained to be the same value for all spectra. In each case, F-tests were used to determine whether the addition of complexity to a model improved the fit sufficiently to better describe the spectra.

The only models for which only the power law normalisation was allowed to vary were the two-component models, i.e. those containing a power law plus a constant (hot gas) component or the partial covering model. Only for these models can simple changes in the normalisation of the power law change the hardness ratio.

The simplest model fitted was a power law with the photon index and normalisation allowed to vary with luminosity (model 1 in Table 3). The next simplest set of models consisted of an absorbed power law, including models in which the absorbing column or the photon index were tied between spectra (models 2-4). The next were a pair of models consisting of an absorbed power law plus a hot gas model, for which the normalisation of the power law was free to vary and the photon index was either free to vary or tied between spectra; all parameters of the hot gas model (i.e. temperature and normalisation) were tied, as it was assumed to be constant (models 56). Also fitted was a set of models consisting of a power law absorbed by an ionised absorber (absori), in which the normalisation of the power law and either the photon index, ionisation state, absorbing column or all three were free to vary between spectra, with the remaining parameters tied (models 8-11). These spectral models were

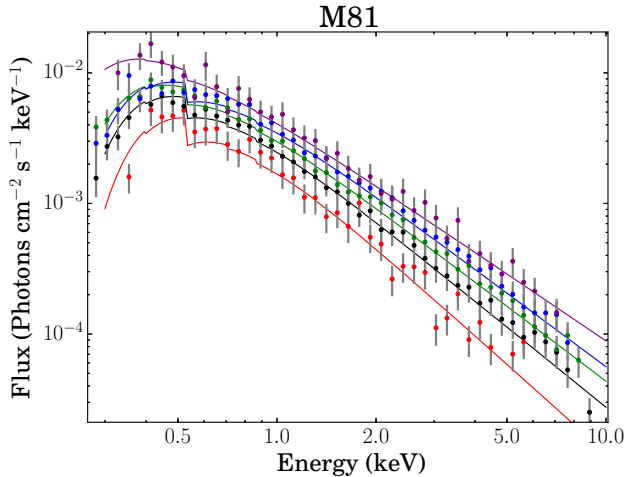


Figure 6. A sample of the flux-binned spectra of M81, fitted with the best-fitting spectral model (see Table 4). Error bars show the one-sigma confidence levels.

fitted to all 14 objects with flux-binned spectra; the results of these fits are in Tables 4 and Table 5.

Objects whose spectra were not well fitted by any of these models were also fitted with a set of models consisting of a power law and a partially-covering absorber (pcfabs) in which, in addition to the normalisation of the power law, either the photon index, absorbing column or covering fraction, the absorbing column *and* the covering fraction, or all three were free to vary (models 12-17). These objects were also fitted with a set of similar models with the addition of a hot gas component, whose parameters were tied between spectra (models 18-23). The results of these fits are in Tables 6 and Table 7.

In addition, NGC 1068 was fitted with a model consisting of a power law with a neutral absorber plus a Gaussian, to account for excess emission at ~ 6.7 keV which is likely to be due to an iron fluorescence line (model 7) (see Section A). The results of these fits are also in Table 7.

The data from the remaining 11 AGN, for which there were not enough data to fit multiple flux-binned spectra, were instead combined to produce a single, total spectrum for each object. These total spectra were fitted in the same fashion as the flux-binned spectra. As only one spectrum was fitted in each case, all parameters were free to vary in all models (except the galactic absorbing column and redshift). Table 8 shows the results of these fits.

Table 9 summarises the best-fitting spectral model for each of the objects for which flux-binned spectra could be produced.

5.1 M81 (NGC 3031)

As the most extensively observed object to show harder-when-brighter behaviour, the spectra of M81 were studied in the greatest detail. The soft component of M81 in particular, extrapolated from its colour-colour plots (see section 4), was derived in order to be able to draw conclusions about similar sources in the sample. Fig. 6 shows a sample of the spectra from M81, covering the full observed flux range.

The X-ray spectrum of M81 is well described by

a simple power law absorbed by the Galactic absorbing column of $7.2 \times 10^{21} \text{ cm}^{-2}$. This is consistent with the many previous shorter-term X-ray studies of M81 (e.g. Elvis & Van Speybroeck 1982; Swartz et al. 2003; Markoff et al. 2008); past studies discovered narrow features attributed to high-ionisation emission lines including Fe lines (e.g. Ishisaki et al. 1996; Pellegrini et al. 2000; Page et al. 2003, 2004), but these are not detectable in the *Swift* data.

The variability in the spectral data is well described by changes in Γ alone; no extra spectral components other than the Galactic absorption in the direction of M81 are required. If the spectrum is assumed to be absorbed by an additional neutral absorber, the variability in the spectral data is equally well described by changes in Γ with the absorbing column fixed or by changes in the absorbing column with a fixed Γ . As these models require an extra component and do not provide a better fit, it is, however, unlikely to be a better description of the data.

If Γ is held constant, we require that the absorbing column decreases as the luminosity rises. In the case of NGC 1365 (Connolly et al. 2014), which has complex luminosity-dependent absorption, greatly in excess of the Galactic column in its direction, such a model is readily explained in terms of a luminosity-dependent wind. However, for M81 there is no evidence in the total summed spectrum for any absorption in excess of the Galactic column. No previous spectral studies have found evidence for such an excess column. As the model with variable absorption requires an additional variable absorbing column in addition to the fixed Galactic column, we consider it less likely than the model of variable Γ , which has one parameter fewer.

Spectral models including the constant component extrapolated from the colour-colour plots (see section 4) were also tested; the component was found not to make a significant enough contribution to the spectrum to account for the variability. The inclusion of this constant component in a model consisting of a power law and a neutral absorber, with a fixed photon index, gave significantly worse fit ($\chi^2_{\text{R}} = 1.15$).

In addition to the constant component extrapolated from the colour-colour plots, we also separately test a model consisting of a constant hot gas (mekal) component together with a power law with varying normalisation but fixed photon index and fixed absorption. In this model, the parameters of the hot gas component are tied to be the same between spectra, but allowed to vary, in order to test whether any significant constant soft component can be found in this way. This model fits the data approximately as well as the model of an absorbed power law with varying photon index. As the photon index is free to vary between flux-binned spectra in the model without the hot gas component, it has more free parameters (i.e. is more complex). However an F-test shows that the simple power law with variable Γ is preferred to the constant- Γ model with a hot component ($f = 2.26$, $p = 3.30 \times 10^{-4}$). Similarly, if the model with a hot gas component in which the photon index is constant is compared to the same model but with the photon index allowed to vary between flux-binned spectra, an f-test shows that the model in which Γ is variable is preferred ($f = 7.78$, $p = 1.27 \times 10^{-29}$) and the varying-photon index model is therefore overwhelmingly preferred; this model is also statistically preferable to the simple absorbed power

N	Description	Xspec Description	Free Parameters
1	Simple power law	pow	Γ
2	Power law with neutral absorber	wabs*pow	Γ
3	Power law with neutral absorber	wabs*pow	N_H
4	Power law with neutral absorber	wabs*pow	N_H, Γ
5	Power law with neutral absorber and hot gas	mekal + (wabs*pow)	-
6	Power law with neutral absorber and hot gas	mekal + (wabs*pow)	Γ
7	Power law with neutral absorber, Gaussian and hot gas	mekal + (wabs*(pow + gauss))	Γ
8	Power law with ionised absorber	absori*pow	Γ
9	Power law with ionised absorber	absori*pow	N_H
10	Power law with ionised absorber	absori*pow	ξ
11	Power law with ionised absorber	absori*pow	N_H, ξ, Γ
12	Partially covered power law	pcfabs*pow	-
13	Partially covered power law	pcfabs*pow	Γ
14	Partially covered power law	pcfabs*pow	N_H
15	Partially covered power law	pcfabs*pow	CF
16	Partially covered power law	pcfabs*pow	N_H, CF
17	Partially covered power law	pcfabs*pow	N_H, CF, Γ
18	Partially covered power law and hot gas	mekal + pcfabs*pow	-
19	Partially covered power law and hot gas	mekal + pcfabs*pow	Γ
20	Partially covered power law and hot gas	mekal + pcfabs*pow	N_H
21	Partially covered power law and hot gas	mekal + pcfabs*pow	CF
22	Partially covered power law and hot gas	mekal + pcfabs*pow	N_H, CF
23	Partially covered power law and hot gas	mekal + pcfabs*pow	N_H, CF, Γ

Table 3. A description of the series of models applied successively to the spectra of each AGN. All models also included the ‘wabs’ model of neutral absorption set to the Galactic absorption column in the direction of each AGN. The free parameters, which can vary between spectra, are shown as symbols: Γ (photon index), N_H (absorbing column), ξ (ionisation parameter) and CF (covering fraction). In all cases the normalisations of the power law was free to vary. In models involving a mekal component, its normalisation was always tied to be the same value in all spectra of a given source.

Xspec Model	pow		wabs*pow				wabs*pow +mekal				wabs*(pow + gauss) + mekal			
Model No.	1		2		3		4		5		6		7	
Free Parameters	χ^2_R	DoF	χ^2_R	DoF	χ^2_R	DoF	χ^2_R	DoF	χ^2_R	DoF	χ^2_R	DoF	χ^2_R	DoF
NGC 1052	2.09	162	2.11	161	2.17	161	2.13	159	1.42	161	1.41	159	1.0743	430
NGC 1068	2.69	436	2.58	435	2.58	435	2.59	431	1.62	437	1.61	433		
NGC 3031	1.01	5902	1.01	5901	1.03	5901	1.01	5874	1.01	5927	0.98	5899		
NGC 3147	0.73	125	0.70	124	0.72	124	0.70	122	0.73	124	0.71	122		
NGC 3227	1.17	1094	1.10	1093	1.57	1093	1.09	1082	1.52	1102	1.08	1091		
NGC 3998	1.40	225	1.39	224	1.69	224	1.42	200	1.63	271	1.42	247		
NGC 4051	2.04	784	2.05	783	2.07	783	2.11	774	1.25	790	1.10	781		
NGC 4151	2.11	703	2.11	702	2.62	702	2.13	696	1.29	707	1.31	695		
NGC 4388	1.92	260	1.93	259	1.92	259	1.94	256	1.17	261	1.17	258		
NGC 4395	1.15	1373	1.15	1372	1.30	1372	1.17	1351	1.31	1392	1.15	1371		
NGC 4486	3.01	261	1.83	260	1.82	260	1.83	257	1.02	261	1.02	258		
NGC 4579	1.09	201	1.10	200	1.09	200	1.11	198	1.00	200	1.00	198		
NGC 5548	1.66	8659	1.46	8658	1.43	8658	1.43	8617	1.15	8697	1.11	8656		

Table 4. The reduced χ^2 values, χ^2_R , and number of degrees of freedom (DoF) of the best fit with models 1-7 to each of the sources. In each case, the free parameters are indicated by Γ (photon index) and N_H (absorbing column). The best fitting model for each source is highlighted in bold.

law, despite its higher level of complexity ($f = 76.0$, $p = 2.48 \times 10^{-33}$). The integrated flux of the extrapolated constant component is within a factor of 2 of that of the hot gas component in the best-fitting model of the full spectrum, and therefore likely to be the same component, though perhaps not well recovered. The data therefore require a constant hot gas component, but it does not contribute to the spectrum enough to explain the overall spectral variability. It is therefore most likely that the observed spectral variability is driven by changes to Γ .

The top-left panel in Fig. 7 shows how Γ changes with increasing flux for the best-fitting model to M81 (model 6).

Γ shows a clear anticorrelation with the luminosity of the source, well fitted by a linear model (see Table 10). Significantly, the same anticorrelation is seen in all models in which Γ is free to vary, regardless of the presence of a hot gas component and whether or not the absorbing column was also left free to vary, strengthening still more the evidence that intrinsic variability of the photon index is required to explain the spectral variability of M81. This anticorrelation between Γ and luminosity is therefore found to be the cause of the observed harder-when-brighter behaviour in M81.

Xspec Model	absori*pow							
Model No.	8		9		10		11	
Free Parameters	Γ		ξ		N_H		Γ, ξ, N_H	
	χ_R^2	DoF	χ_R^2	DoF	χ_R^2	DoF	χ_R^2	DoF
NGC 1052	1.42	159	1.51	159	1.85	159	1.48	155
NGC 1068	2.37	433	2.59	433	2.59	433	2.56	425
NGC 3147	0.71	122	0.72	122	0.73	122	0.72	118
NGC 3031	1.01	5900	1.03	5900	1.03	5900	1.02	5846
NGC 3227	1.05	1091	1.27	1091	1.31	1091	1.17	1069
NGC 3998	1.47	247	1.64	247	1.82	247	1.78	199
NGC 4051	1.15	781	1.14	781	1.13	781	1.11	763
NGC 4151	2.02	701	1.78	701	1.96	701	1.16	689
NGC 4388	2.38	258	1.92	258	1.93	258	1.66	252
NGC 4395	1.03	1370	1.08	1370	1.06	1370	1.01	1328
NGC 4486	1.82	259	1.81	259	1.84	259	1.86	253
NGC 4579	1.09	198	1.18	198	1.08	198	1.08	194
NGC 5548	0.96	8656	0.95	8656	0.96	8656	0.94	8574

Table 5. The reduced χ^2 values, χ_R^2 , and number of degrees of freedom (DoF) of the best fit with models 8-11 to each of the sources. In each case, the free parameters are indicated by Γ (photon index), N_H (absorbing column) and ξ (ionisation state). The best fitting model for each source is highlighted in bold.

Xspec Model	pcfabs*pow																	
Model No.	12		13		14		15		16		17							
Free Parameters	Γ										N_H		CF		N_H, CF		Γ, N_H, CF	
	χ_R^2	DoF	χ_R^2	DoF	χ_R^2	DoF	χ_R^2	DoF	χ_R^2	DoF	χ_R^2	DoF	χ_R^2	DoF	χ_R^2	DoF	χ_R^2	DoF
NGC 1052	1.11	162	1.01	160	1.08	160	1.03	160	1.00	158	0.99	156						
NGC 1068	2.24	438	2.24	434	2.25	434	2.26	434	2.27	430	2.28	426						
NGC 4151	1.23	708	1.20	702	1.22	702	1.16	702	1.15	696	1.13	690						

Table 6. The reduced χ^2 values, χ_R^2 , and number of degrees of freedom (DoF) of the best fit with models 12-17 to the sources not well fit by models 1-11. In each case, the free parameters are indicated by Γ (photon index), N_H (absorbing column) and CF (covering fraction). The best fitting model for each source is highlighted in bold.

5.2 The Palomar Swift Sample of AGN

Details on the spectral fitting of individual AGN in the sample are given in Appendix A, along with examples of the spectra (Figs. A, A2).

5.2.1 Flux-Binned Spectral Modelling

A simple power law, either not absorbed, absorbed by a neutral absorber, or absorbed by an ionised absorber, fitted the spectra of 4 of the 13 flux-binned sources well; in all 4 cases, a varying photon index was required to account for spectral variability. Two of the sources were, however, better fit when the absorbing column and ionisation state of the absorber were also allowed to vary.

The addition of a constant hot gas component to the absorbed power law was required in 6 of the 13 flux-binned sources (including M81). The spectral variability of only 1 of these 6 sourced can only be explained by variability in the normalisation of a power law with constant Γ together with this constant hot gas component. The other 5 sources required Γ to also be free to vary. Allowing the absorber to vary (i.e. absorbing column and ionisation state where the absorber was ionised) did not improve the fit in any of these sources.

A more complex model was required for a good fit to the remaining 3 of the 13 flux-binned objects - NGC 1052, NGC 4151 and NGC 4388. NGC 1052 and NGC 4151 both required a partial covering absorber; Allowing the photon index to vary did not improve the fit in this model for NGC

1052, whilst in NGC 4151 a varying photon index was required, but a varying absorbing column and covering fraction were also needed. NGC 4388 required a two-component model consisting of two power laws, one of which is absorbed by a neutral absorber. The normalisations of the two power laws were correlated in this model, implying both originate from the central source. In this model, allowing the photon index to vary did not improve the fit.

The results of the fits to the spectra of NGC 1068, NGC 4151, NGC 4388 were not included in subsequent analysis, as they were deemed unphysical (see Appendix A).

Fig. 7 shows plots of the value of Γ as a function of flux of the 9 objects observed by *Swift* whose best-fitting models required variations in Γ (including M81), plus NGC 7213 for comparison. The data are fitted with linear models in the same manner as were the hardness data described in Section 3. The results of these fits are shown in Table 10. Of these 10 objects, 9 show a clear trend of changing Γ with luminosity. 6 of the objects showed a negative correlation, 3 showed a positive correlation and 1 shows no clear correlation. The best linear fits to NGC 3998 and NGC 5548 (harder-when-brighter), NGC 3227, NGC 4051 and NGC 4395 (softer-when-brighter) all have high χ_R^2 values, due to the larger degree of scatter in the measured values of Γ for these systems. The Pearson correlation coefficients for these systems still show them to be fairly strongly correlated, however. All of the objects' behaviours are consistent with that implied by their hardness ratio vs. flux plots, except for NGC 5548; however the behaviour of its hardness ratio with changing flux is not as simple as the others (as described above) and

Xspec Model	pcfabs*pow + mekal											
Model No.	18		19		20		21		22		23	
Free Parameters	–		Γ		N_{H}		CF		N_{H}, CF		$\Gamma, N_{\text{H}}, \text{CF}$	
	χ^2_{R}	DoF	χ^2_{R}	DoF	χ^2_{R}	DoF	χ^2_{R}	DoF	χ^2_{R}	DoF	χ^2_{R}	DoF
NGC 1068	1.12	436	1.10	432	1.11	432	1.12	432	1.12	428	1.12	424
NGC 4151	1.11	706	1.11	700	1.12	700	1.07	700	1.06	694	1.03	688

Table 7. The reduced χ^2 values, χ^2_{R} , and number of degrees of freedom (DoF) of the best fit with models 18-23 to the sources not well fit by models 1-17. In each case, the free parameters are indicated by Γ (photon index), N_{H} (absorbing column) and CF (covering fraction). The best fitting model for each source is highlighted in bold.

spectral modelling shows that it possesses complex, variable absorption (Kaastra et al. 2014).

The data therefore imply that a significant fraction of objects which displayed harder-when-brighter behaviour do show hardening of their intrinsic spectra, i.e. a decrease in photon index, Γ , with increasing luminosity. All of the objects showing softer-when brighter showed softening of their intrinsic spectra (i.e. an increase in Γ) with increasing luminosity. One can therefore conclude that the behaviour of the hardness ratio with changing luminosity is a reasonable predictor of the behaviour of the spectral slope of the underlying power law, and that it is likely that a similar fraction of the remaining objects which showed harder-when-brighter behaviour in their hardness ratio vs. count rate plots, whose data did not allow spectral fitting, would also possess intrinsic hardening.

5.2.2 Total Spectral Modelling

Spectral fitting was also carried out on the total spectra of the 11 objects for which there was sufficient data to produce plots of hardness ratio vs. luminosity, but not sufficient data for flux-binned spectral fitting. All of the available good-quality data on each of these objects was summed and fitted in the same manner as for the flux-binned spectra. The results of this spectral analysis are presented in Table 8. Of these 11 objects, 7 possessed evidence for either complex absorption, i.e. variable partial-covering absorbers, or strong contamination, e.g. from hot gas. The remaining 4 objects possessed spectra which can be described by simple power laws, with evidence of absorption in 3 of the objects. These four objects also show harder-when-brighter behaviour in the plots of hardness ratio vs. luminosity (Fig. 2). The spectral modelling therefore shows the harder-when-brighter behaviour of these objects due to changes in their photon indices and/or absorbing columns which are correlated with luminosity.

The harder-when-brighter behaviour seen in 6 of the 7 objects with more complex spectra could be caused by variations in parameters other than γ , i.e. the absorption, ionisation state and/or covering fraction. NGC 4321, whose hardness ratio behaviour with increasing luminosity did not follow any simple pattern, has a complex spectrum which could not be well fitted by any of the models. As we have limited spectral data in all of these cases, we cannot be sure of the cause of their behaviour without further data to allow multi-epoch or flux-binned spectral modelling.

6 SUMMARY & DISCUSSION

We have analysed the long-term observations with *Swift* of a sample of 24 nearby AGN from the Palomar sample in order to determine the reason for their variability. This study concentrates on trying to determine long-term systematic trends rather than investigating short-term fluctuations which may not be representative of the overall underlying behaviour. The main results of this study are:

- From examination of simple hardness ratios, we find that 18 of the AGN show hardening of their X-ray spectra with increasing luminosity, 2 showed softening of their X-ray spectra with increasing luminosity, 2 showed more complex behaviour although generally softening with increasing luminosity and the remaining 2 did not show any correlation between their spectral hardness and luminosity.

- There are 13 AGN for which there were sufficient data for flux-binned spectral fits to be made. Of these, NGC 1068, NGC 4395, NGC 4151 and NGC 5548 show complex absorption, i.e. variable partial-covering absorbers, in their spectra, both in our *Swift* observations and in previous observations (see notes on individual sources), which makes it difficult to determine the true cause of the hardness variability. The other 8 are fit by relatively simple power law plus absorption models, making interpretation of the hardness variations simpler. Of these 8, NGC 3227 and NGC 4051 show increasing Γ with increasing luminosity. Of the other 6, NGC 3031 (M81) and NGC 3998, for which there are a large number of observations, all show a decrease of Γ with increasing luminosity. NGC 1052, NGC 3147 and NGC 4579, for which there are fewer observations, show the same behaviour. All of the AGN which show decreasing Γ with increasing luminosity have values of $L_{\text{x}}/L_{\text{Edd}}$ of $< 2 \times 10^{-4}$. The 2 AGN which show increasing Γ with increasing luminosity have values of $L_{\text{x}}/L_{\text{Edd}}$ of $> 10^{-3}$.

- For the 11 objects for which spectral analysis could only be carried out on a summed spectrum of all their data, 3 were found to have spectra which could be described by a simple absorbed power law - NGC 3226, NGC 3628 and NGC 5806. The spectral modelling therefore implies that the harder-when-brighter behaviour of these 3 objects can only be due either to changes in their photon indices which are negatively correlated with luminosity, or due to changes in absorption which are negatively correlated with luminosity. As with the harder-when-brighter objects whose spectra were flux-binned, the value of $L_{\text{x}}/L_{\text{Edd}}$ is $< 2 \times 10^{-4}$ for NGC 3226. The masses of NGC 3628 and NGC 5806 have not been determined, so their Eddington luminosities could not be calculated, but their low X-ray luminosities imply that they are very likely to have values of $L_{\text{x}}/L_{\text{Edd}}$ which are $< 2 \times 10^{-4}$; They would have to have very low masses of

Xspec Model	pow		wabs*pow		absori*pow		wabs*pow + mekal		pcfabs*pow		pcfabs*pow + mekal		wabs*(pow+gauss) + mekal	
	χ^2_R	DoF	χ^2_R	DoF	χ^2_R	DoF	χ^2_R	DoF	χ^2_R	DoF	χ^2_R	DoF	χ^2_R	DoF
NGC 315	3.80	26	3.28	26	4.92	24	1.02	24						
NGC 2655	10.37	47	9.76	46	4.65	44	2.51	44	3.36	45	1.15	43		
NGC 3226	2.64	31	0.90	30	0.97	28								
NGC 3628	2.66	16	0.88	15	1.02	13								
NGC 4258	6.77	56	6.90	55	3.27	52	2.70	53	2.91	54	1.03	52		
NGC 4321	3.71	11	2.56	10	5.04	8	1.62	7						
NGC 4472	13.36	46	4.84	45	6.37	45	1.03	43						
NGC 4736	1.69	82	1.55	81	1.75	79	0.97	79						
NGC 5194	12.25	134	7.13	133	12.27	131	1.80	131	9.75	132	1.46	131	1.18	127
NGC 5806	1.27	16	1.16	15	1.45	13								
NGC 7331	2.63	26	2.69	25	2.79	23	0.83	23						

Table 8. Results of spectral fitting to the total spectra of those objects with too little data for flux binning. All models included a neutral absorber fixed at Galactic absorbing column in that direction.

Source	Best-Fitting		Best-Fitting Parameters				
	Spectral Model	$N_H(10^{22}\text{cm}^{-2})$	Γ	kT (keV)	CF	Ξ	
NGC 315	1	0.78	1.94	0.56	-	-	
NGC 1052	13	8.60	1.37 – 1.70	-	0.91	-	
NGC 1068	7	55.7	2.90 – 3.06	0.67	0.95	-	
NGC 2655	23	20.5	1.35	0.57	0.95	-	
NGC 3031	6	0	1.69-2.05	0.55	-	-	
NGC 3147	2	-	1.35 – 1.58	-	-	-	
NGC 3226	4	0.54	2.57	-	-	-	
NGC 3227	8	0.13	1.43 – 1.65	-	-	0.045	
NGC 3628	4	0.35	1.36	-	-	-	
NGC 3998	1	-	1.87 – 2.50	-	-	-	
NGC 4051	6	0	1.35 – 1.97	0.20	-	-	
NGC 4151	23	3.01 – 5.07	0.76 – 1.20	0.23	0.76 – 0.95	-	
NGC 4258	23	9.89	1.66	0.60	0.95	-	
NGC 4321	6	1.51	4.46	0.43	-	-	
NGC 4388	5	26.3	1.05 – 1.24	0.62	-	-	
NGC 4395	8	2.17	0.91 – 1.60	-	-	215.16	
NGC 4472	6	0.81	3.83	0.74	-	-	
NGC 4486	5	0.45	2.68	1.52	-	-	
NGC 4579	5	0.01	1.67	0.52	-	-	
NGC 4736	6	0.055	1.48	0.35	-	-	
NGC 5194	7	0	0.7	0.60	-	-	
NGC 5806	4	0.057	1.65	-	-	-	
NGC 5548	11	0.64 – 1.43	1.09 – 1.40	-	-	7.46 – 35.88	
NGC 7331	6	0.075	1.37	0.37	-	-	

Table 9. The best-fitting spectral model for each of the sources, and the values of the parameters which were free to vary (excluding normalisations, which were always free but are not included). See Table 3 for a description of each model.

Object	χ^2/DoF	Gradient	Intercept	Pearson coefficient	Behaviour when brighter
M81	0.95	$-0.14^{+0.02}_{-0.024}$	$2.16^{+0.04}_{-0.05}$	-0.89	harder
NGC 1052	1.70	$-0.52^{+0.36}_{-0.53}$	$2.07^{+0.52}_{-0.37}$	-0.96	harder
NGC 3147	0.58	$-1.77^{+1.46}_{-1.94}$	$1.87^{+0.44}_{-0.31}$	-0.91	harder
NGC 3227	2.81	$0.048^{+0.02}_{-0.01}$	$1.33^{+0.07}_{-0.08}$	0.73	softer
NGC 3998	3.11	$-0.34^{+0.10}_{-0.11}$	$2.42^{+0.10}_{-0.09}$	-0.74	harder
NGC 4051	13.22	$0.31^{+0.09}_{-0.09}$	$0.82^{+0.21}_{-0.22}$	0.65	softer
NGC 4395	10.21	$0.21^{+0.02}_{-0.02}$	$1.13^{+0.02}_{-0.02}$	0.63	softer
NGC 4579	1.59	$-0.49^{+1.52}_{-1.48}$	$2.14^{+1.07}_{-1.16}$	-0.83	undetermined
NGC 5548	19.46	$-0.13^{+0.02}_{-0.02}$	$1.63^{+0.06}_{-0.05}$	-0.50	harder
NGC 7213	0.23	$-0.06^{+0.02}_{-0.02}$	$1.98^{+0.04}_{-0.04}$	-0.91	harder

Table 10. The reduced χ^2 and best-fit parameters (with one-sigma errors) for linear fits to the photon index vs. flux plots of each object (see Fig. 7). The Pearson correlation coefficient for each object is also shown.

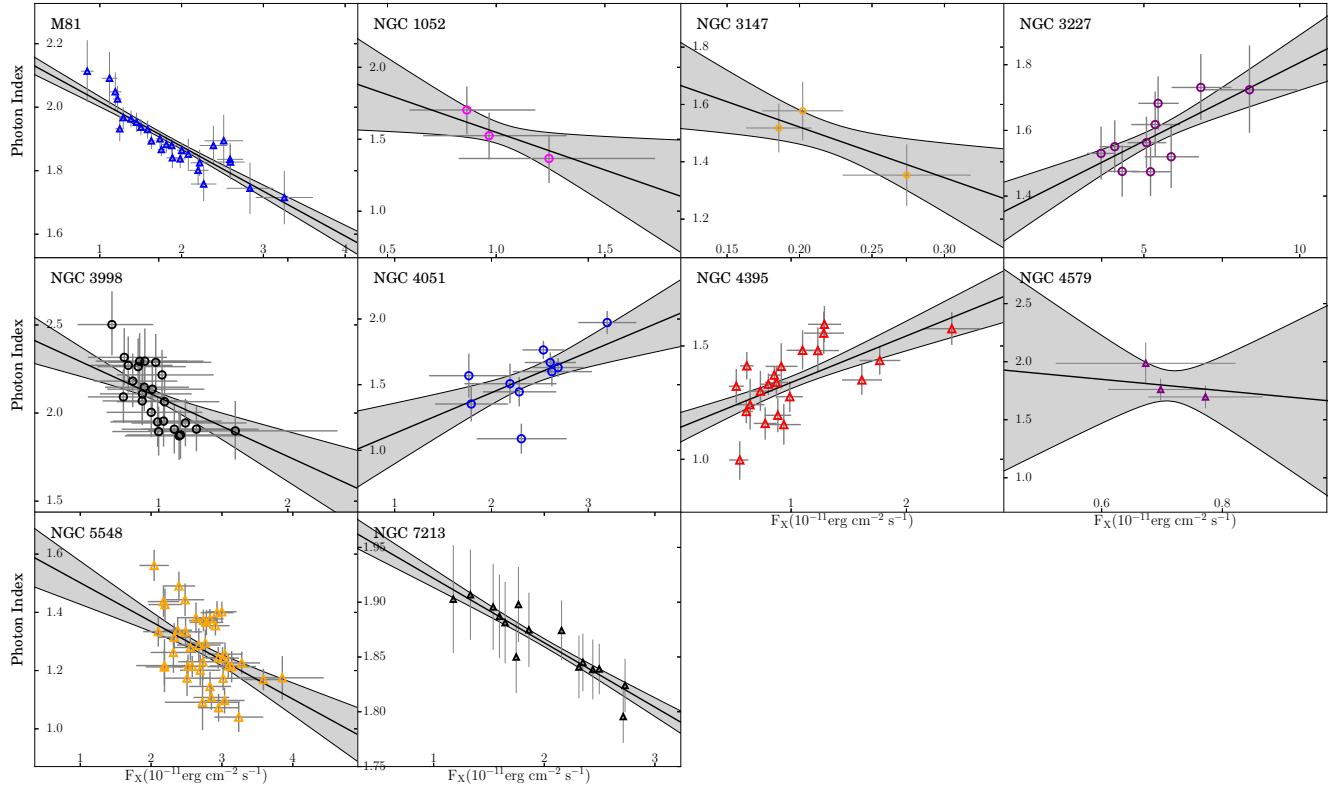


Figure 7. Plots of the photon index Γ against the X-ray flux of each of the sources for which flux-binned spectral fitting was carried out, using the best-fitting model in each case. The 0.5 – 10keV flux is used in all cases except for NGC 3998, for which the 3 – 20keV *RXTE* flux is used. Error bars show the one-sigma confidence levels. The data are fitted with linear models; the best-fitting model is shown in black and the one-sigma error regions of each fit are shown in grey.

$< 6.3 \times 10^5 M_{\odot}$ and $< 3.2 \times 10^5 M_{\odot}$ respectively in order to have values of L_x/L_{Edd} which are $> 2 \times 10^{-4}$.

6.1 Correlations between Photon Index and Luminosity

We find that below L_x/L_{Edd} of 2×10^{-4} , all AGN with well measured spectral variability show a decrease in Γ with increasing luminosity (i.e. hardening of the underlying spectral slope). Above that value of L_x/L_{Edd} , Γ increases with L_x . For an assumed bolometric correction factor of $L_{\text{bol}}/L_x = 16$ (Ho 2008; Constantin et al. 2009), this value would correspond to $L_{\text{bol}}/L_{\text{Edd}}$ (i.e. \dot{m}_{Edd}) of 3.2×10^{-3} . NGC 5548 and NGC 4395 both show complex behaviour in their hardness ratios (see Fig. 3), with the largest scatter in our sample and are both known to possess complex variable absorption (Kaastra et al. 2014; Nardini & Risaliti 2011) which is likely to complicate the interpretation of their observed behaviour. Previous studies (e.g. Sobolewska & Papadakis 2009) have shown an increase in Γ with increasing Luminosity within individual AGN at high accretion rates, with the exception of NGC 5548.

In Fig. 8 we show all of the measurements of Γ for our sample, excluding those for which we had reason to distrust the measured values of Γ (see Appendix A). We also plot the fits to Γ from previous samples of LLAGN by Constantin et al. (2009) and, at higher accretion rates, from Shemmer et al. (2006).

The variations of Γ in M81 and NGC 7213, which are relatively bright sources with well measured spectra, follow the trend of Constantin et al. (2009) fairly well. However, the individual observations of some objects show a steeper variation with luminosity. This difference might be real or it might be due to an unknown systematic effect, e.g. over-subtraction of the hard background spectrum. If the steeper gradients are not a systematic effect, they could be explained in a number of ways. A weak constant soft component which is not resolved in the spectrum would artificially enhance the flattening of the photon index with increasing luminosity, as its relative contribution to the soft end of the spectrum decreases. Absorption variability could also enhance the change in the photon index, but the amount of absorption would be required to increase with increasing luminosity, which is hard to explain physically; it is perhaps possible if a higher luminosity leads to an increase in the wind-driving ability of the system, due to e.g. a hotter disk or more ionised matter available for line-driving, but the timescales for this mechanism to lead to an increase in absorption are likely to be too long to explain the observed spectral changes (see e.g. Proga 2007). Finally, the difference in the rate of change of Γ with luminosity between individual AGN and sample averages could be real. We note that the spread of data points around the best fit relationship for both Constantin et al. (2009) and Shemmer et al. (2006) is very large. Thus although the change in Γ within any individual AGN is determined only by the change in accretion rate and any subse-

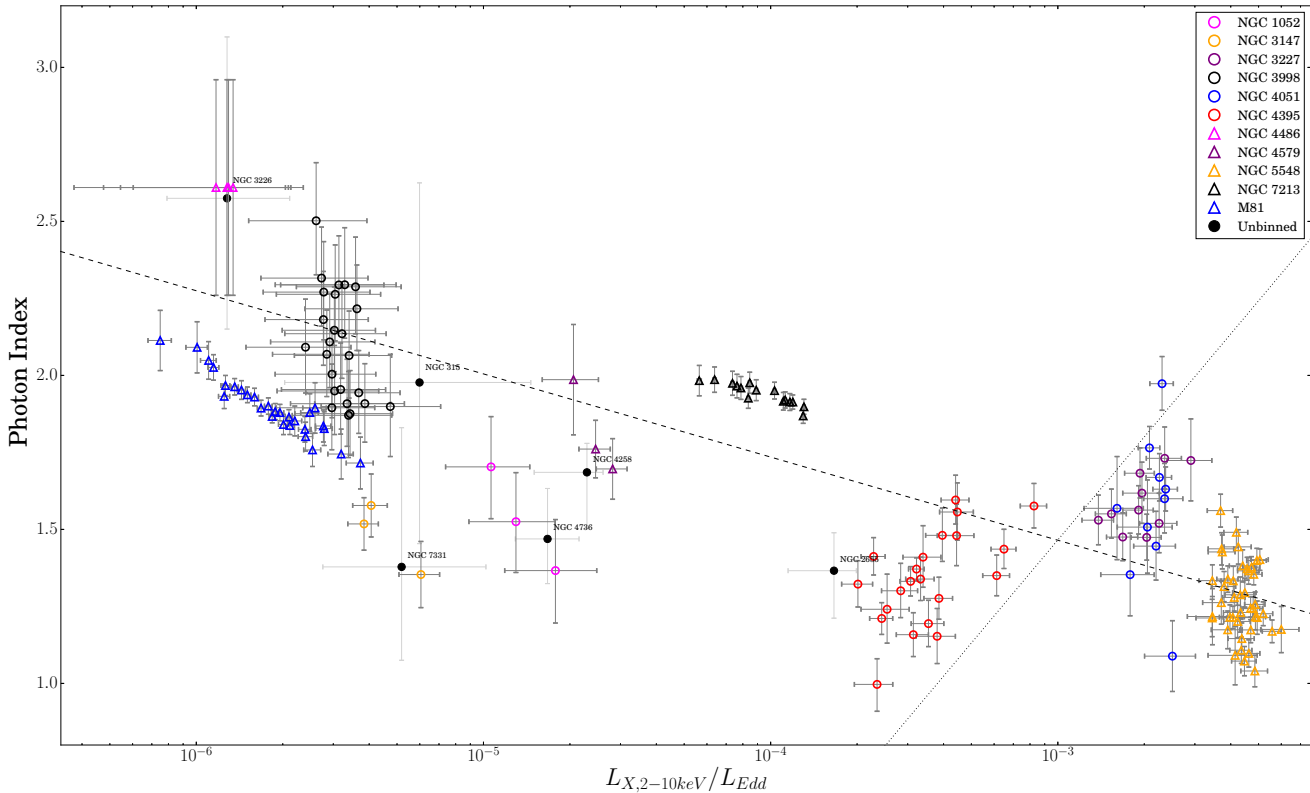


Figure 8. Plot of Γ against $L_{X,2-10\text{keV}}/L_{\text{Edd}}$ (as a proxy for \dot{m}_{Edd}), for all of the Palomar *Swift* AGN for which values of the photon index could be constrained, and NGC 7213 (data from Emmanoulopoulos et al. (2012)). In the cases of NGC 3998 and NGC 7213, the flux was scaled from the 3.3-20 keV flux according to the best-fitting model. Objects which did not have enough data to be flux-binned are plotted individually in grey and labelled. The dashed line is the fit to a sample of LLAGN from (Constantin et al. 2009), the dotted line is the fit to a sample of higher Eddington rate radio-quiet AGN from (Shemmer et al. 2006). Error bars show the one-sigma confidence levels. The black hole masses and distances used to calculate the Eddington luminosities and the X-ray luminosities are shown in Table 11.

quent related changes, e.g. change in absorption, the spread of Γ within samples can also be affected by changes related to the black hole mass. For example mass-related changes in disc temperature at a given Eddington ratio could lead to differences in the relative importance of disc seed photons and coronal synchrotron seed photons (Shakura & Sunyaev 1973; M^cHardy et al. 2014).

All of the AGN with $L_x/L_{\text{Edd}} < 2 \times 10^{-4}$ are seen to broadly lie on a similar track, indicating that a similar physical process is responsible for the behaviour of all of the objects in the sample. The rate of change in Γ with luminosity in these lower accretion rate objects is relatively similar in all harder-when-brighter sources, implying similarities between all of the objects in the physical causes of this anticorrelation. Some of the sources show similar gradients to that of the Constantin et al. (2009) relationship, but several show slightly steeper gradients. The accuracy of the measurement of the distances and black hole masses of the AGN is limited in some cases and consequently the values of L_x/L_{Edd} may be offset for some objects. It should be noted that, in addition to the aforementioned caveats, the bolometric correction could also vary between objects, meaning that their position on this plot is not precisely correct.

For the softer-when-brighter sources, NGC 4051 and NGC 3227 are broadly consistent with the trend shown by

Shemmer et al. (2006) and can be explained by the standard model of cooling of the corona with increasing accretion rate and disc seed photon flux. As discussed above, the behaviour of NGC 4395 and NGC 5548 is more complex.

The shift from a negative to a positive correlation between Γ and \dot{m}_{Edd} , and therefore from harder-when-brighter to softer-when-brighter behaviour, is probably due to a transition of the dominant seed photon population for X-ray production, from synchrotron or cyclo-synchrotron emission from the X-ray emitting corona itself, or from a hot inner flow/ADAF, to black body photons from a surrounding accretion disc (e.g. Skipper et al. 2013; Sobolewska et al. 2011).

The same synchrotron self-Compton emission process which dominates the X-ray emission from coronae at low accretion rates could also come from a jet; harder-when-brighter behaviour due to a Γ - \dot{m}_{Edd} anticorrelation is common in blazars (e.g. Krawczynski et al. 2004; Gliozzi et al. 2006; Zhang et al. 2006), e.g. due to shock acceleration of electrons in a jet producing both higher energy synchrotron seed photons and higher energy (inverse) Compton scattering. This mechanism has been proposed to explain e.g. the spectral evolution of the BHXRB XTEJ1550-564 as it transitions from the ‘soft state’ towards the ‘hard state’ (Russell et al. 2010; Emmanoulopoulos et al. 2012). There

Object	Log(L _R , 5GHz) (ergs s ⁻¹)	Log(L _{X,2-10keV}) (ergs s ⁻¹)	Log(L _X /L _R)	L _{bol} (ergs s ^{-s})	Eddington Ratio (L _{bol} /L _{Edd})	Log(Mass) (M _⊙)	Dist (Mpc)
NGC 1052	35.4 ^a	39.8	4.40	42.2 ^p	7.3 × 10 ⁻⁵	8.3 ^r	19.0
NGC 1068	36.9 ^b	39.8	2.90	45.0 ^r	5.0 × 10 ⁻¹	7.2 ^r	12.25
NGC 2655	36.3 ^d	41.2	4.91	42.2 [*]	3.6 × 10 ⁻⁴	7.8 ^{ee}	24.4
NGC 3031	36.8 ^c	41.9	5.10	41.5 ^m	3.5 × 10 ⁻⁵	7.9 ^t	3.63
NGC 3147	38.0 ^d	40.4	2.40	41.4 [*]	5.3 × 10 ⁻⁶	8.8 ^{bb}	43.7
NGC 315	39.7 ^d	41.6	1.87	42.6 [*]	6.1 × 10 ⁻⁵	8.9 ^r	51.3
NGC 3226	37.3 ^d	40.4	3.10	41.4 [*]	2.0 × 10 ⁻⁵	8.2 ^{bb}	26.35
NGC 3227	36.3 ^d	41.0	4.70	43.1 ^s	1.3 × 10 ⁻²	7.6 ^x	20.85
NGC 3628	39.2 ^e	40.2	1.00	41.2 [*]	-	-	11.25
NGC 3998	38.2 ^d	41.4	3.20	43.5 ^r	3.2 × 10 ⁻⁴	9.0 ^r	18.65
NGC 4051	37.0 ^b	41.8	4.80	42.6 ^s	1.9 × 10 ⁻²	6.2 ^x	15.5
NGC 4151	39.8 ^f	44.1	4.30	44.0 ^s	1.8 × 10 ⁻²	7.7 ^y	16.2
NGC 4258	35.8 ^d	40.4	4.57	43.5 ^r	6.1 × 10 ⁻³	7.6 ^z	7.56
NGC 4321	35.7 ^g	39.7	4.01	43.5 ⁿ	3.6 × 10 ⁻²	6.8 ^{bb}	16.0
NGC 4388	39.0 ^b	43.1	4.10	43.7 ^s	6.5 × 10 ⁻²	6.8 ^{bb}	18.55
NGC 4395	34.8 ^d	42.0	7.20	41.4 ^s	3.9 × 10 ⁻²	5.6 ^{aa}	4.3
NGC 4472	36.5 ^d	40.3	3.80	41.5 [*]	1.5 × 10 ⁻⁶	8.8 ^{ff}	15.9
NGC 4486	38.9 ^d	42.6	3.70	43.8 [*]	1.6 × 10 ⁻⁴	9.5 ^{bb}	16.5
NGC 4579	37.7 ^d	42.2	4.50	42.0 ^o	1.1 × 10 ⁻⁴	7.9 ^{bb}	20.5
NGC 4736	37.6 ^f	39.9	2.3	41.1 [*]	5.6 × 10 ⁻⁵	7.0 ^{cc}	4.86
NGC 5194	36.7 ^f	39.2	2.46	43.8 ^r	5.7 × 10 ⁻²	7.0 ^{bb}	7.94
NGC 5548	36.1 ^b	40.8	4.70	44.1 ^s	1.6 × 10 ⁻²	7.8 ^y	92.50
NGC 5806	-	39.9	-	40.9 [*]	-	-	26.1
NGC 7331	37.2 ^e	39.8	2.61	40.8 [*]	2.3 × 10 ⁻⁵	7.6 ^{dd}	14.55
NGC 7213	38.7 ⁱ	42.1 ^k	3.40	43.0 ⁿ	7.4 × 10 ⁻⁴	8.0 ^r	22.00
Sag A*	32.6 ^j	33.4 ^l	0.80	41.0 ^o	1.0 × 10 ⁻⁵	6.6 ^v	8.33 × 10 ⁻³

Table 11. Radio luminosities at 5GHz and 2-10 keV X-ray luminosities, Eddington ratios, masses and distances for all 24 AGN, plus NGC 7213 and Saggiarius A* for comparison. The ratios between the luminosities of each object are also given. Data taken from: (a) Horiuchi et al. (2004), (b) Gallimore et al. (2004), (c) Perez-Olea & Colina (1996), (d) Nagar et al. (2005), (e) Sramek (1975), (f) Laurent-Muehleisen et al. (2008), (g) Filho et al. (2006), (h) Irwin et al. (2015), (i) Bell et al. (2011), (j) Zhao et al. (2001), (k) Emmanoulopoulos et al. (2012), (l) Baganoff et al. (2003), (m) Ho et al. (1996), (n) Ptak (2004), (o) Lewis & Eracleous (2006), (p) Skipper (2013), (q) Starling et al. (2005), (r) Woo & Urry (2002), (s) Vasudevan & Fabian (2009), (t) Devereux et al. (2003), (u) Walsh et al. (2012), (v) Gillessen et al. (2009), (w) McHardy et al. (2014), (x) Denney et al. (2010), (y) Bentz et al. (2006), (z) Herrnstein et al. (2005), (aa) Peterson, Bentz, Desroches, Filippenko, Ho, Kaspi, Laor, Maoz, Moran, Pogge & Quillen (Peterson et al.), (bb) Merloni et al. (2003) (cc) Hernández-García et al. (2014) (dd) Filho et al. (2004), (ee) Gu & Cao (2009), (ee) Panessa & Giroletti (2013), (ff) Ho (1999), * - using bolometric correction, x16. Dashes indicate that no measurement known to the authors exists.

is no evidence yet for highly relativistic outflows in LLAGN, such as are seen in blazars, but weak jets are detected (e.g. Marti-Vidal et al. 2011) and models for such jets (e.g. Markoff et al. 2008) can explain the observed X-ray spectral variability.

One further explanation for harder-when-brighter behaviour is a hot outflowing corona above an X-ray illuminated untruncated disc (Sobolewska et al. 2011), in which the seed photons are from the disc. In this model, the seed photon flux is limited by relativistic beaming of the outflowing corona. At higher luminosities, a higher outflow velocity decreases the illumination of the disc and therefore the seed photon population, softening the spectrum. However, this model predicts that at the lowest luminosities there should be a strong reflection component from an untruncated disk, whilst many of the low-luminosity sources in this study, including M81, show little evidence for reflection, but good evidence for an ADAF flow and a truncated disc from the x-ray spectrum and the presence of radio emission (Ptak 2004; Brenneman et al. 2009; Markoff et al. 2008; Young & Nowak 2007; Nowak et al. 2010).

6.2 AGN and BHXR State Analogues

Both the harder-when-brighter relation and the softer-when-brighter relation are also well established in black hole X-ray binaries (BHXRBs) and have been observed both in samples of single-epoch observations and in multi-epoch observations of individual objects (e.g. Kalemci et al. 2004; Yuan et al. 2007; Yamaoka et al. 2005). As in samples of AGN, they are seen to switch from a positive correlation to a negative correlation between Γ and \dot{m} , and therefore from harder-when-brighter to softer-when-brighter behaviour, when \dot{m}_{Edd} increases above a critical value, \dot{m}_{crit} . This value is identified as $\sim 10^{-2} \dot{m}_{\text{Edd}}$ from samples of AGN (Wu & Gu 2008), and directly observed in the BHXR Cyg X-1, (Axelsson et al. 2008; Skipper et al. 2013; Skipper & McHardy 2016).

Previous studies have looked for changes in the photon index with luminosity of individual LLAGN before (Younes et al. 2011; Hernández-García et al. 2013, 2014, e.g.), but been unsuccessful; our ability to detect changes in the photon index more easily is likely due to the larger flux-ranges covered by our data. As the amplitude of the change in Γ is proportional to the change in the luminosity of the system, a large flux range is essential. A large amplitude of variability is therefore also important, as changes in

Γ will be hard to find in systems with very low variability regardless of the timescales covered. Methodological differences, such as the use of flux-binning, may also contribute, but we believe these effects to be less significant.

For BHXRBs, the transition from harder-when-brighter to softer-when-brighter takes place entirely within the hard state Wu & Gu (2008); Skipper & McHardy (2016) and softer-when-brighter behaviour continues throughout the hard-intermediate state, at accretion rates below that of the change to the soft state. Thus all of the AGN in our sample are probably analogues to either hard state or hard-intermediate state BHXRBs. Thus LINERS, with accretion rates $< \sim 10^{-2} \dot{m}_{\text{Edd}}$ are analogues to hard state BHXRBs whilst Seyferts may be analogues to either higher accretion rate hard state, or to hard-intermediate state BHXRBs.

A so-called ‘fundamental plane’ relationship between X-ray luminosity, radio luminosity and black hole mass has previously been shown for samples of AGN and BHXRBs (e.g. Merloni et al. 2003; Koering et al. 2006). In Table 11 we give the X-ray luminosities for our sample from our observations together with radio luminosities and black hole masses from the literature. We do not show the ‘fundamental plane’ derived from the data in Table 11, but note that there is no obvious distinction between Seyferts and LINERS, indicating again that they are parts of a continuous distribution. The X-ray luminosities are from our present data and the radio are from the literature.

The discovery that the individual variations in Γ in the *Swift* AGN sample are consistent with previous fits to samples of AGN as well as similar studies showing the variability in Γ of individual BHXRBs therefore adds strong evidence the idea that AGN are scaled-up analogues of the BHXRBs. Based on the present data, which are the best data in which a harder-when-brighter correlation may be found in individual AGN, we suggest that this behaviour is very common amongst LLAGN.

ACKNOWLEDGMENTS

SDC thanks the STFC for support under a studentship and IMcH thanks the STFC for support via grant ST/G003084/1. We note our appreciation to Tom Dwelly, who wrote our original Swift data analysis system. We thank the anonymous referee for constructive comments which greatly strengthened the paper.

REFERENCES

Antonucci R. R. J., S. M. J., 1985, *ApJ*, 297, 621
 Arnaud K., 1996, *Astronomical Data Analysis Software Systems V*, 101, 17
 Awaki H., Koyama K., Kunieda H., Takano S., Tawara Y., 1991, *ApJ*, 366, 88
 Axelsson M., Hjalmarsdotter L., Borgonovo L., Larsson S., 2008, *A&A*, 490, 253
 Baganoff F. K., Maeda Y., Morris M., Bautz M. W., Brandt W. N., Cui W., Doty J. P., Feigelson E. D., Garmire G. P., Pravdo S. H., Ricker G. R., Townsley L. K., 2003, *ApJ*, 591, 891

Bauer F. E., Arevalo P., Walton D. J., Koss M. J., Puccetti S., Gandhi P., Stern D., Alexander D. M., Balokovic M., Boggs S. E., Brandt W. N., Brightman M., Christensen F. E., Comastri A., Craig W. W., Del Moro A., Hailey C. J., Harrison F. a., Hickox R., Luo B., Markwardt C. B., et al. 2014, *ApJ*, 812, 116
 Bell M. E., Tzioumis T., Uttley P., Fender R. P., Arévalo P., Breedt E., McHardy I., Calvelo D. E., Jamil O., Körding E., 2011, *MNRAS*, 411, 402
 Bentz M. C., Denney K. D., Cackett E. M., Dietrich M., Fogel J. K. J., Ghosh H., Horne K., Kuehn C. a., Minezaki T., Onken C. a., Peterson B. M., Pogge R. W., Pronik V. I., Richstone D. O., Sergeev S. G., Vestergaard M., Walker M. G., Yoshii Y., 2006, *ApJ*, 651, 775
 Beuchert T., Markowitz A., Krauss F., Miniutti G., Longinotti a. L., Guainazzi M., Elvis M., Miyaji T., Hiriart D., Agudo I., Kadler M., Wilms J., Dauser T., García J., 2015, *A&A*, 584, 82
 Brenneman L. W., Weaver K. a., Kadler M., Tueller J., Marscher A., Ros E., Zensus A., Kovalev Y., Aller M., Aller H., Irwin J., Kerp J., Kaufmann S., 2009, *ApJ*, 698, 528
 Brightman M., Baloković M., Stern D., Arévalo P., Ballantyne D. R., Bauer F. E., Boggs S. E., Craig W. W., Christensen F. E., Comastri A., Fuerst F., Gandhi P., Hailey C. J., Harrison F. a., Hickox R. C., Koss M., LaMassa S., Puccetti S., Rivers E., Vasudevan R., et al. 2015, *ApJ*, 805, 41
 Cameron D. T., McHardy I., Dwelly T., Breedt E., Uttley P., Lira P., Arevalo P., 2012, *MNRAS*, 422, 902
 Cao Y., Kasliwal M. M., Arcavi I., Horesh A., Hancock P., Valenti S., Cenko S. B., Kulkarni S. R., Gal-Yam A., Gorbikov E., Ofek E. O., Sand D., Yaron O., Graham M., Silverman J. M., Wheeler J. C., Marion G. H., Walker E. S., Mazzali P., Howell D. A., Li K. L., Kong a. K. H., Bloom J. S., Nugent P. E., Surace J., et al. 2013, *ApJ*, 775, 7
 Connolly S. D., 2015, *PoS(SWIFT 10)*, 1, 131
 Connolly S. D., McHardy I. M., Dwelly T., 2014, *MNRAS*, 440, 3503
 Constantin A., Green P., Aldcroft T., Kim D.-W., Haggard D., Barkhouse W., Anderson S. F., 2009, *ApJ*, 705, 1336
 Dahlem M., Heckman T. M., Fabbiano G., , *ApJ*, 442, 49
 Denney K. D., Peterson B. M., Pogge R. W., Adair A., Atlee D. W., Au-Yong K., Bentz M. C., Bird J. C., Brokofsky D. J., Chisholm E., Comins M. L., Dietrich M., Doroshenko V. T., Eastman J. D., Efimov Y. S., Ewald S., Ferbey S., Gaskell C. M., Hedrick C. H., Jackson K., Klimanov S. A., Klimek E. S., Kruse A. K., et al. 2010, *ApJ*, 721, 715
 Devereux N., Ford H., Tsvetanov Z., Jacoby G., 2003, *AJ*, 125, 1226
 Dewangan G. C., Griffiths R. E., Di Matteo T., Schurch N. J., 2004, *ApJ*, 607, 788
 Dudik R. P., Satyapal S., Gliozzi M., Sambruna R. M., 2005, *ApJ*, 620, 113
 Elvis M., Risaliti G., Nicastro F., Miller J. M., Fiore F., Puccetti S., 2004, *ApJ*, 615, 25
 Elvis M., Van Speybroeck L., 1982, *ApJ*, 257L, 51
 Emmanoulopoulos D., Papadakis I. E., McHardy I. M., Arévalo P., Calvelo D. E., Uttley P., 2012, *MNRAS*, 424, 1327

- Emmanoulopoulos D., Papadakis I. E., Nicastro F., McHardy I. M., 2013, MNRAS, 429, 3439
- Esin A. A., McClintock J. E., Narayan R., 1997, ApJ, 489, 865
- Filho M. E., Barthel P. D., Ho L. C., 2006, A&A, 451, 71
- Filho M. E., Fraternali F., Markoff S., Nagar N. M., Barthel P. D., Ho L. C., Yuan F., 2004, A&A, 418, 429
- Gallimore J. F., Baum S. a., O’Dea C. P., 2004, ApJ, p. 38
- Gallo L. C., Lehmann I., Pietsch W., Boller T., Brinkmann W., Friedrich P., Grupe D., 2006, MNRAS, 365, 688
- George I. M., Turner T. J., Netzer H., Nandra K., Mushotzky R. F., Yaqoob T., 1998, ApJS, 114, 73
- Ghisellini G., Haardt F., Matt G., 1994, MNRAS, 267, 743
- Ghisellini G., Maraschi L., Tavecchio F., 2009, MNRAS, 396, L105
- Gillessen S., Eisenhauer F., Trippe S., Alexander T., Genzel R., Martins F., Ott T., 2009, ApJ, 692, 1075
- Gliozzi M., Sambruna R. M., Jung I., Krawczynski H., Horan D., Tavecchio F., 2006, ApJ, 646, 61
- Gondoin P., Orr A., Siddiqui H., 2004, A&A, 420, 905
- González-Martín O., Masegosa J., Márquez I., Guainazzi M., Jiménez-Bailón E., 2009, A&A, 506, 1107
- González-Martín O., Masegosa J., Márquez I., Guerrero M. a., Dultzin-Hacyan D., 2006, A&A, 460, 45
- Gu M., Cao X., 2009, MNRAS, 399, 349
- Hernández-García L., González-Martín O., Márquez I., Masegosa J., 2013, A&A, 556, 47
- Hernández-García L., González-Martín O., Masegosa J., Márquez I., 2014, A&A, 569, 26
- Herrnstein J. R., Moran J. M., Greenhill L. J., Trotter A. S., 2005, ApJ, 629, 719
- Ho L. C., 1999, ApJ, 516, 672
- Ho L. C., 2008, ARA&A, 46, 475
- Ho L. C., Filippenko A. V., Sargent W. L. W., 1996, ApJ, 462, 183
- Ho L. C., Filippenko A. V., Sargent W. L. W., 1997a, ApJS, 112, 315
- Ho L. C., Filippenko A. V., Sargent W. L. W., 1997b, ApJ, 487, 568
- Horiuchi S., Fomalont E. B., Taylor W. K., Scott A. R., Lovell J. E. J., Moellenbrock G. A., Dodson R., Murata Y., Hirabayashi H., Edwards P. G., Gurvits L. I., Shen Z.-Q., 2004, ApJ, 616, 110
- Irwin J. a., Henriksen R. N., Krause M., Wang Q. D., Wiegert T., Murphy E. J., Heald G., Perlman E., 2015, ApJ, 809, 172
- Ishisaki Y., Makishima K., Iyomoto N., Hayashida K., Inoue H., Mitsuda K., Tanaka Y., Uno S., Kohmura Y., Mushotzky R. F., Petre R., Serlemitsos P. J., Terashima Y., 1996, PASJ, 48, 237
- Iwasawa K., Tanaka Y., Gallo L. C., 2010, MNRAS, 514, 58
- Kaastra J. S., Kriss G. A., Cappi M., Mehdipour M., Petrucci P.-O., Steenbrugge K. C., Arav N., Behar E., Bianchi S., Boissay R., Branduardi-Raymont G., Chamberlain C., Costantini E., Ely J. C., Ebrero J., Di Gesu L., Harrison F. a., Kaspi S., Malzac J., De Marco B., et al. 2014, Science, 345, 64
- Kalemci E., Tomsick J. a., Buxton M. M., Rothschild R. E., Pottschmidt K., Corbel S., Brocksopp C., Kaaret P., 2004, A&A, 622, 508
- Keck M. L., Brenneman L. W., Ballantyne D. R., Bauer F., Boggs S. E., Christensen F. E., Craig W. W., Dauser T., Elvis M., Fabian a. C., Fuerst F., García J., Grefenstette B. W., Hailey C. J., Harrison F. a., Madejski G., Marinucci A., Matt G., Reynolds C. S., Stern D., Walton D. J., Zoghbi A., 2015, ApJ, 806, 149
- Koerding E., Falcke H., Corbel S., 2006, A&A, 456, 439
- Krawczynski H., Hughes S. B., Horan D., Aharonian F., Aller M. F., Aller H., Boltwood P., Buckley J., Holder J., Horns D., Kurtanidze O. M., Marscher A. P., Coppi P., Fossati G., Go N., Nikolashvili M., Remillard R. A., Sadun A., Schro M., 2004, ApJ, 601, 151
- Lamer G., Hardy I. M. M., Uttley P., Jahoda K., 2003, MNRAS, 338, 323
- Laurent-Muehleisen S. A., Kollgaard R. I., Ryan P. J., Feigelson E. D., Brinkmann W., Siebert J., 2008, A&A, 122, 235
- Lewis K. T., Eracleous M., 2006, ApJ, 642, 711
- Loewenstein M., Mushotzky R., Angelini L., Arnaud K., Quataert E., 2001, ApJ, 555, 21
- Maccarone T. J., Gallo E., Fender R., 2003, MNRAS, 345, 19
- Markoff S., Nowak M., Young A., Marshall H. L., Canizares C. R., Krips M., Petitpas G., Scho R., Bower G. C., Ray A., Muno M., Gallagher S., Hornstein S., 2008, ApJ, 681, 905
- Marti-Vidal I., Marcaide J. M., Alberdi A., Prez-Torres M. A., Ros E., Guirado J. C., 2011, A&A, 533, 111
- Matsumoto Y., Fukazawa Y., Nakazawa K., Iyomoto N., Makishima K., 2001, PASJ, 53, 475
- Merloni A., Heinz S., Di Matteo T., 2003, MNRAS, 345, 1057
- McHardy I. M., Cameron D. T., Dwelly T., Connolly S., Lira P., Emmanoupolous D., Gelboud J., Breedt E., Arevalo P., Uttley P., 2014, MNRAS, 444, 1469
- McHardy I. M., Papadakis I. E., Uttley P., 1998, Nuclear Phys. B, 69, 509
- Nagar N. M., Falcke H., Wilson a. S., 2005, A&A, 435, 521
- Narayan R., 1994, ApJ, 428, L13
- Nardini E., Risaliti G., 2011, MNRAS, 417, 3571
- Nemmen R. S., StorchiBergmann T., Yuan F., Eracleous M., Terashima Y., Wilson A. S., 2006, ApJ, 643, 652
- Nowak M., Markoff S., Young A., 2010, MmSAI, 81, 414
- Page M. J., Breeveld A. A., Soria R., Wu K., Mason K. O., Starling R. L. C., Zane S., 2003, A&A, 400, 145
- Page M. J., Soria R., Zane S., Wu K., Starling R. L. C., 2004, A&A, 422, 77
- Panessa F., Giroletti M., 2013, MNRAS, 432, 1138
- Pellegrini S., Cappi M., Bassani L., Malaguti G., Palumbo G. G. C., Persic M., 2000, A&A, 353, 447
- Perez-Olea D. E., Colina L., 1996, ApJ, 468, 191
- Peterson B. M., Bentz M. C., Desroches L.-b., Filippenko A. V., Ho L. C., Kaspi S., Laor A., Maoz D., Moran E. C., Pogge R. W., Quillen A. C., , ApJ
- Ponti G., Miniutti G., Cappi M., Maraschi L., Fabian A. C., Iwasawa K., 2008
- Proga D., 2007, ASPC, 373, 267
- Ptak A., 1999, ApJS, 120, 179
- Ptak A., 2004, ApJ, 606, 173
- Ptak A., Yaqoob T., Serlemitsos P. J., Kunieda H., Terashima Y., 1996, ApJ, 459, 542
- Ptak A., Yaqoob T., Serlemitsos P. J., Mushotzky R., Otani C., 1994, ApJ, 436, 31

Puccetti S., Fiore F., Risaliti G., Capalbi M., Elvis M., Nicastro F., 2007, *MNRAS*, 377, 607
 Risaliti G., Elvis M., Nicastro F., 2002, *ApJ*, 571, 234
 Roberts T. P., Schurch N. J., Warwick R. S., 2001, *MNRAS*, 324, 737
 Russell D. M., Maitra D., Dunn R. J. H., Markoff S., 2010, *MNRAS*, 405, 1759
 Seth A., Agüeros M., Lee D., BasuZych A., 2008, *ApJ*, 678, 116
 Shakura N. I., Sunyaev R. A., 1973, *A&A*, 24, 337
 Shemmer O., Brandt W. N., Netzer H., Maiolino R., Kaspi S., 2006, *ApJ*, 646, L29
 Skipper C. J., 2013, PhD thesis, University of Southampton
 Skipper C. J., Mc Hardy I. M., Maccarone T. J., 2013, *MNRAS*, 434, 574
 Skipper C. J., McHardy I. M., 2016, *MNRAS* (submitted)
 Sobolewska A., Papadakis I. E., 2009, *MNRAS*, 399, 1597
 Sobolewska M. a., Papadakis I. E., Done C., Malzac J., 2011, *MNRAS*, 417, 280
 Sramek R., 1975, *ApJ*, 80, 771
 Starling R. L. C., Page M. J., Branduardi-Raymont G., Breeveld A. A., Soria R., Wu K., 2005, *MNRAS*, 356, 727
 Steenbrugge K. C., Kaastra J. S., Crenshaw D. M., Kraemer S. B., Arav N., George I. M., Liedahl D. a., van der Meer R. L. J., Paerels F. B. S., Turner T. J., Yaqoob T., 2005, *A&A*, 434, 569
 Swartz D. A., Ghosh K. K., Mccollough M. L., Pannuti T. G., Tennant A. F., Wu K., 2003, *ApJ*, 144, 213
 Taylor R. D., Uttley P., Hardy I. M. M., Hardy M., 2003, *MNRAS*, 342, 31
 Terashima Y., Iyomoto N., Ho L. C., Ptak A., 2002, *ApJ*, 139, 1
 Vasudevan R. V., Fabian a. C., 2009, *MNRAS*, 392, 1124
 Walsh J. L., van den Bosch R. C. E., Barth A. J., Sarzi M., 2012, *ApJ*, 753, 79
 Wang J., Fabbiano G., Elvis M., Risaliti G., Mazzarella J. M., Howell J. H., Lord S., Processing I., 2009, *ApJ*, 294
 Weaver K. A., Wilson A. S., Henkel C., Braatz J. A., 1999, *ApJ*, 520, 130
 Woo J., Urry C. M., 2002, *ApJ*, 579, 530
 Wu Q., Gu M., 2008, *ApJ*, 682, 212
 Yamada S., Itoh T., Makishima K., Nakazawa K., 2009, *PASJ*, 61, 309
 Yamaoka K., Uzawa M., Arai M., Yamazaki T., Yoshida A., 2005, *ChJAS*, 5, 273
 Yang Q.-x., Xie F.-g., Yuan F., Zdziarski A. a., Gierli M., Ho L. C., Yu Z., 2015, *MNRAS*, 447, 1692
 Younes G., Porquet D., Sabra B., Reeves J. N., 2011, *A&A*, 530, 149
 Young A. J., Nowak M. A., 2007, *ApJ*, 669, 830
 Yuan F., Taam R. E., Misra R., Wu X., Xue Y., 2007, *ApJ*, 658, 282
 Zhang Y. H., Treves A., Maraschi L., Bai J. M., Liu F. K., 2006, *ApJ*, 637, 699
 Zhao J.-H., Bower G. C., Goss W. M., 2001, *ApJ*, 547, L29

APPENDIX A: NOTES ON SPECTRAL FITTING OF INDIVIDUAL PALOMAR AGN

The following section contains details on the results of spectral fitting for each of the 24 AGN in our sample.

• NGC 315

Only a single summed spectrum of NGC 315 could be produced from the available *Swift* data. Our best-fitting model consists of an absorbed power law, plus a hot gas component ($\chi^2_{\text{R}} = 1.02$). Previous spectral modelling of NGC 315 has employed very similar models (e.g Matsumoto et al. 2001; Terashima et al. 2002; Younes et al. 2011). The photon index we measure is very similar to that found by Matsumoto et al. (2001) and Younes et al. (2011) ($\Gamma = 1.94$; slightly higher than that found by Terashima et al. (2002)).

• NGC 1052

Three flux-binned spectra could be produced from the available *Swift* data of NGC 1052. We found that a single partial coverer provided a very good fit to the spectra. A fairly good fit is obtained when all the parameters are tied ($\chi^2_{\text{R}} = 1.11$). However, allowing Γ , the absorbing column or the covering fraction to produces a fit which is statistically better in each case ($f = 9.5$ and $p = 1.3 \times 10^{-4}$, $f = 3.5$ and $p = 3.3 \times 10^{-2}$, $f = 8.0$ and $p = 4.7 \times 10^{-4}$ respectively). The best fit is obtained when only Γ is left free ($\chi^2_{\text{R}} = 1.01$). Models in which both the absorbing and column and the covering fraction are free to vary but Γ is tied, or in which all three are free to vary, provided lower χ^2 values, but the added complexity is not required statistically when compared to the model in which only Γ is free to vary between flux-binned spectra ($f = 1.7$ and $p = 0.19$, $f = 1.6$ and $p = 0.186$ respectively). Previous studies by Weaver et al. (1999) and Hernández-García et al. (2013), using *ASCA*, *Chandra* and *XMM-Newton* data, also concluded that the spectrum was heavily absorbed by one or more partial-coverers.

For the best-fitting model, in which the absorber is constant and Γ is free to vary between flux-binned spectra, Γ is anticorrelated with the flux. Furthermore, the same anticorrelation is seen in our spectral fits when the absorbing column is allowed to vary as well as the photon index. The values of Γ found are between those found by Weaver et al. (1999) and by Hernández-García et al. (2013) $\Gamma = 1.37 - 1.70$ for similar models, though Hernández-García et al. (2013) attribute the primary cause of spectral changes in NGC 1052 to variations in the absorbing column, not the photon index. As the source displays harder-when-brighter behaviour, if the spectral variations are caused by absorption variation alone this absorption must be negatively correlated with the luminosity of the system, as in e.g. NGC 1365 (Connolly et al. 2014).

• NGC 1068

Three flux-binned spectra could be produced from the available *Swift* data of NGC 1068. The components of our best-fitting model to the spectra required an absorbed power law, a hot gas component for contamination from the host. This is consistent with previous modelling of the source, which used similar models (e.g. Bauer et al. 2014; Brightman et al. 2015). However, the photon index we obtain is higher than that found with previous data from e.g. *NuStar* which included higher energies than those detected by *Swift*, though indices of > 2 have been found. NGC 1068 is widely thought to be a Compton-thick AGN, making the intrinsic emission difficult to model (Antonucci & S. 1985; Ghisellini et al. 1994; Brightman et al. 2015), as the degree of absorption could not be constrained with the energy range

of *Swift*, the flux extracted from this spectrum was much lower than the true value. For these reasons, NGC 1068 was not included in the subsequent discussion of spectral variability behaviour.

- **NGC 2655**

Insufficient *Swift* data was available to produce multiple flux-binned spectra for NGC 2655, so a single-summed spectrum was produced. We also find a partial covering model to be the best-fitting to the *Swift* data ($\chi^2_{\text{R}} = 1.15$), when combined with an additional hot gas component. Previous work on NGC 2655 has also required a partial covering model, and a hot gas component in some cases (e.g. Terashima et al. 2002; González-Martín et al. 2009). The best-fitting model has a very hard photon index ($\Gamma = 1.35$), but this is consistent with what others have found previously (Terashima et al. 2002).

- **NGC 3147**

Three flux-binned spectra of NGC 3147 were produced from the *Swift* data. We find the best-fitting model to the *Swift* data to be a simple power law for which Γ was allowed to vary ($\chi^2_{\text{R}} = 0.73$). Previous modelling of the spectrum of NGC 3147 has also shown a lack of any strong absorption (e.g. Ptak et al. 1996). As the *Swift* data are already slightly over-fitted by this model ($\chi^2_{\text{R}} < 1$), we assume that more complex models are incorrect, despite producing lower χ^2 values. We find similar values of the photon index to those found by (Ptak et al. 1996) ($\Gamma = 1.35 - 1.58$). This model show a reduction in Γ with increasing intrinsic luminosity of the system.

- **NGC 3226**

Only a single summed spectrum of NGC 3226 could be produced from the *Swift* data. We find that the spectrum is very well-fitted by a power law and a neutral absorber ($\chi^2_{\text{R}} = 0.90$). Past studies disagree somewhat as to whether the best-fitting model for the spectrum of NGC 3226 is bremsstrahlung or a simple power law (e.g. González-Martín et al. 2009; Gondoin et al. 2004; Younes et al. 2011), but previous work agrees on the presence of a neutral absorber. We find a high value for the photon index, but with large uncertainties ($\Gamma = 2.57 \pm 0.42$); Gondoin et al. (2004) and Younes et al. (2011) find value which is lower, but which agree with ours within our errors.

- **NGC 3227**

Sufficient *Swift* data of NGC 3227 was available to produce 10 flux-binned spectra. The best-fitting model to the *Swift* data consisted of a power law and an ionised absorber, with Γ free to vary but all parameters of the absorber tied ($\chi^2_{\text{R}} = 1.07$), which is statistically superior to a neutral absorber ($f = 16.3$ and $p = 1.1 \times 10^{-7}$). Previous spectral modelling of NGC 3227 has also shown its spectrum to be absorbed by an ionised absorber (George et al. 1998; Ptak et al. 1994), though some more recent studies have used more complex models involving multiple ionised absorbers and a reflection component (e.g. Beuchert et al. 2015). The parameters of our best-fitting model show a positive correlation between the photon index and the intrinsic luminosity of the source, consistent with Sobolewska & Papadakis (2009), who also found the same correlation and range of photon indices ($\Gamma = 1.43 - 1.65$) in the 2 – 10keV band.

- **NGC 3628**

Only a single summed spectrum of NGC 3628 could be

produced from the *Swift* data. We found a power law with a neutral absorber to be best-fitting to the *Swift* data. Previous studies have found the same spectral model to be best-fitting (Dahlem, Heckman & Fabbiano Dahlem et al.; González-Martín et al. 2009), with a similarly low photon index ($\chi^2_{\text{R}} = 1.36$) to that found in our best-fitting model.

- **NGC 3998**

As there were few *Swift* data available for NGC 3998, we instead used the *RXTE* data from Skipper (2013), for which a large number of flux-binned spectra could be produced. The *RXTE* data are of quite low S/N, as NGC 3998 is a very faint source. The spectrum can be fitted reasonably well by a power law absorbed by the galactic absorbing column of $1.05 \times 10^{21} \text{cm}^{-2}$, and shows no excesses which imply that this is not a good model. The fit is not improved by the addition of a further absorber, possibly because the *RXTE* does not extend below 3 keV, so is only sensitive to high absorbing columns. If it is assumed that the spectrum is absorbed and that the source of the spectral variability is changes in absorption instead of a changing Γ , a significantly worse fit is obtained. This is consistent with previous spectral studies of this source (Ptak 2004; Awaki et al. 1991; Younes et al. 2011). The values obtained for the photon index in previous studies are all within the range found in this model ($\Gamma \sim 1.87 - 2.50$). In the best-fitting model, the photon index shows a clear anticorrelation with the intrinsic luminosity of the system. Younes et al. (2011) also found variations in Γ , but had only two observations so could not test for any correlation.

- **NGC 4051**

There were sufficient *Swift* data to produce 10 flux-binned spectra of NGC 4051. We find that absorbed power law plus a hot gas component also fits the *Swift* data well ($\chi^2_{\text{R}} = 1.10$). Previous spectral modelling of NGC 4051 with *XMM-Newton* data has also used an absorbed power law plus a hot gas component (e.g. Ponti et al. 2008). We find that the photon index is positively correlated with the flux, as found previously by Ponti et al. (2008); Sobolewska & Papadakis (2009) with *XMM-Newton* and *RXTE* in the 0.5 – 10keV and 2 – 10keV bands respectively, with the same range of values for the photon index ($\Gamma = 1.35 - 1.97$). This correlation is less clear in the 2 – 10keV band, perhaps due to the absorption variations found by e.g. Lamer et al. (2003); Ponti et al. (2008) making our parameter measurements less accurate over the narrower band.

- **NGC 4151**

There were sufficient *Swift* data to produce 7 flux-binned spectra of NGC 4151. We find a power law plus a neutral partially-covering absorber to be the best-fitting model to the *Swift* data ($\chi^2_{\text{R}} = 1.02$). Previous work has also shown NGC 4151 to be best modelled with these components (e.g. Puccetti et al. 2007; Keck et al. 2015, with *ROSAT*, *NuSTAR* and *Suzaku* respectively). The values of the photon index we find are, however, very low. The large absorbing column and complex, variable absorption are likely to have limited accurate measurement of the underlying spectral index. We therefore exclude the results of the spectral fitting to NGC 4151 from the subsequent discussion.

- **NGC 4258**

Only a single summed spectrum of NGC 4258 could be produced from the available *Swift* data. We find that a

partial covering absorber and a hot gas component is required to obtain a good-fit ($\chi_R^2 = 1.03$), significantly better than a fully-covering absorber ($\chi_R^2 = 1.78$). Previous studies of NGC 4258 have, however, found the spectrum to be best modelled by a simple absorbed power law and a hot gas component (Yamada et al. 2009; Terashima et al. 2002). The value we find for the photon index ($\Gamma = 1.66$) is consistent with that of Terashima et al. (2002) and (Yamada et al. 2009).

- **NGC 4321**

Only a single spectrum of NGC 4321 could be produced from the *Swift* data. We find that an absorbed power law plus a hot gas component is best-fitting ($\chi_R^2 = 1.62$), consistent with previous spectral studies of NGC 4321 (González-Martín et al. 2009; Roberts et al. 2001). In our data, however, the hot gas component from the host is dominant, meaning the underlying spectral index is not well constrained. The results of this spectral fitting are therefore not included in subsequent analysis.

- **NGC 4388**

Sufficient *Swift* data were available to produce 4 flux-binned spectra of NGC 4388. We also obtained a reasonable fit to the *Swift* data with a power law and a neutral absorber ($\chi_R^2 = 1.16$). This model did not require the photon index (or absorption) to vary between flux-binned spectra, though the spectra only cover a small range of fluxes and therefore may not be expected to change significantly. Previous studies have also fitted the spectrum with a model consisting of as absorbed power law (e.g. Elvis et al. 2004; Risaliti et al. 2002). However, we obtain a very low value for the photon index ($\Gamma = 1.10$), which does not agree with the value found in previous studies - together with the high level of absorption ($N_H \sim 3 \times 10^{23} \text{ cm}^{-2}$), which is great enough to affect the majority of the *Swift XRT* energy range, were therefore conclude that the underlying spectrum, and therefore the intrinsic luminosity, of NGC 4388 are not well constrained. The results of the spectral fitting to NGC 4388 are therefore not included in subsequent analysis.

- **NGC 4395**

The large quantity of *Swift* data of NGC 4395 allowed us to produce 22 flux-binned spectra. We find that a model consisting of a power law and an ionised absorber gives a good fit to the *Swift* data. The best-fitting model of the flux-binned spectra requires only the photon index to vary ($\chi_R^2 = 1.03$); although the model in which the ionisation state and absorbing column are free to vary does give a lower χ^2 , the extra complexity is not statically required ($f = 0.31, p = 1.00$). The spectrum has previously been modelled with multiple absorbers with varying ionisation states and absorbing columns (e.g. Iwasawa et al. 2010; Nardini & Risaliti 2011). The lack of a need for variability in the absorption, despite previous work showing absorption variability to be present, is perhaps due to the flux-binning averaging the absorption over the period covered by the data, but this is likely to add scatter to the parameter values. Some of the spectral indices obtained from this fit are very hard ($\Gamma = 0.91 - 1.60$), so absorption variability is not ruled out as the source of spectral variability, however the values are consistent with the values found by Iwasawa et al. (2010), who also found evidence of variations in Γ . Our spectral modelling therefore also implies that there is not any flux dependence in the degree of absorption.

- **NGC 4472**

Spectral modelling of NGC 4472 has been limited due to its very low-luminosity. We find that an absorbed power law fits the spectrum of NGC 4472 very well in conjunction with a hot gas component ($\chi_R^2 = 1.03$) consistent with previous work, which has used a simple power law model (Loewenstein et al. 2001). However, the hot gas component dominates the spectrum in our data due to the low luminosity of the x-ray source, making constraints on the intrinsic spectrum less reliable; we find an unphysically high photon index of $\Gamma = 3.38$. We therefore conclude that the spectral fitting could not reliably find the parameters of the intrinsic spectrum and exclude the results from subsequent analysis.

- **NGC 4486**

Four flux-binned spectra were produced from the available *Swift* data of NGC 4486. We find that a single power law plus a hot gas model gives a good fit to the spectra ($\chi_R^2 = 1.03$). The model in which Γ does not vary is best-fitting, as the model in which Γ varies is not statistically better ($f = 0.1, p = 0.96$), meaning we obtain only a single value for the whole range of luminosities. Previous spectral modelling of NGC 4486 has also mostly used a single, absorbed power law (e.g. González-Martín et al. 2006; Dudik et al. 2005), though some have used more complex, multi-component models (e.g. González-Martín et al. 2009). As the flux range is relatively small, it may be that in reality there are small variations which cannot be successfully resolved in the *Swift* data. The value for the photon index obtained ($\Gamma = 2.68$) is relatively high, but consistent with the value found by (González-Martín et al. 2009) within our errors.

- **NGC 4579**

Three flux-binned spectra were produced from the available *Swift* data of NGC 4486. We find an absorbed powerlaw and a hot gas component to be a good fit ($\chi_R^2 = 1.00$). Previous studies also required an absorbed powerlaw and a hot gas component (González-Martín et al. 2009; Dewangan et al. 2004). We find a range of photon indices very similar to those found by previous studies ($\Gamma = 1.7 - 2.0$). The photon index decreases with increasing luminosity in this model.

- **NGC 4736**

Only a single summed spectrum of NGC 315 could be produced from the available *Swift* data. We find an absorbed power law plus a hot gas component to be the best-fitting to the *Swift* data. Previous studies successfully also model the spectrum of NGC 4736 with an absorbed power law and a hot gas component (e.g. Roberts et al. 2001; Terashima et al. 2002). We find a very similar value for the photon index to previous studies ($\Gamma = 1.45$).

- **NGC 5194**

We find the spectrum of NGC 5194 a heavily absorbed power law with and a Gaussian to be the best fit to the *Swift* data. Previous spectral studies of NGC 5194 have also found it to be well fit by a heavily absorbed power law, with a strong Fe emission line (Terashima et al. 2002; Ptak 1999). As the source is Compton thick, however, we cannot constrain the absorption well with the *Swift* data; we obtain an extremely low photon index ($\Gamma = 0.7$), significantly lower than that found in previous studies. We therefore conclude that both the value of Γ and the x-ray luminosity we obtain are unreliable and consequently do not include the results of the spectral fits to NGC 5194 in subsequent analysis.

- **NGC 5548**

The large quantity of *Swift* data of NGC 5548 allowed us to produce 42 flux-binned spectra. We find that the flux-binned *Swift* data are well-fitted by a single, ionised absorber for which Γ , the absorbing column and the ionisation state are all free to vary ($\chi^2_{\text{R}} = 0.94$). The data are also well fitted by changes in each of these parameters alone, but statistically the model in which they are all free to vary is superior ($f = 3.3$ and $p = 6.9 \times 10^{-21}$, $f = 2.2$ and $p = 5.4 \times 10^{-9}$, $f = 662.7$ and $p = 7.7 \times 10^{-141}$ compared to the models in which only Γ , the absorbing column or the ionisation state were free to vary, respectively). This is consistent with previous studies which have found NGC 5548 possesses complex variable absorption (e.g. Steenbrugge et al. 2005; Kaastra et al. 2014).

In the best-fitting model, there does not appear to be any strong correlation between Γ and the intrinsic luminosity of the x-ray source, though there are hints of a negative correlation. The lack of any correlation being found may be due to the complex, variable absorption adding a large amount of scatter to the measured values, however a previous study by (Sobolewska & Papadakis 2009) with *RXTE* (whose data is less affected by absorption at 3 – 20keV) also did not find any significant correlation between Γ and luminosity in the 2 – 10keV band, with the same scatter in Γ that we find. They also find a higher range of photon indices, further suggesting that the variable absorption in NGC 5548 is affecting the accuracy of our measurements of the photon index.

- **NGC 5806**

Only a single summed spectrum of NGC 5806 could be produced from the available *Swift* data. We find that the *Swift* data for NGC 5806 are best-fitted by an absorbed power law ($\chi^2_{\text{R}} = 1.16$), with a fairly typical photon index of $\Gamma = 1.65$. Although NGC 5806 has been classified as an AGN optically (Seth et al. 2008), there have been no X-ray spectral studies of this object to date; the X-ray data used in this study are taken from observations intended to look at the iPTF13bvn supernova which occurred in NGC 5806 in 2013 (the supernova occurred near the edge of the galaxy and could therefore not have contaminated the spectrum of the nucleus) (Cao et al. 2013).

- **NGC 7331**

Only a single summed spectrum of NGC 7331 could be produced from the available *Swift* data. We find an absorbed power law and a hot gas component to be best-fitting to the *Swift* data. Previous X-ray studies of NGC 7331 employed similar models (González-Martín et al. 2006; Gallo et al. 2006). We find a slightly lower photon index than previous studies, but the value obtained is compatible within our errors ($\Gamma = 1.38 \pm 0.3$).

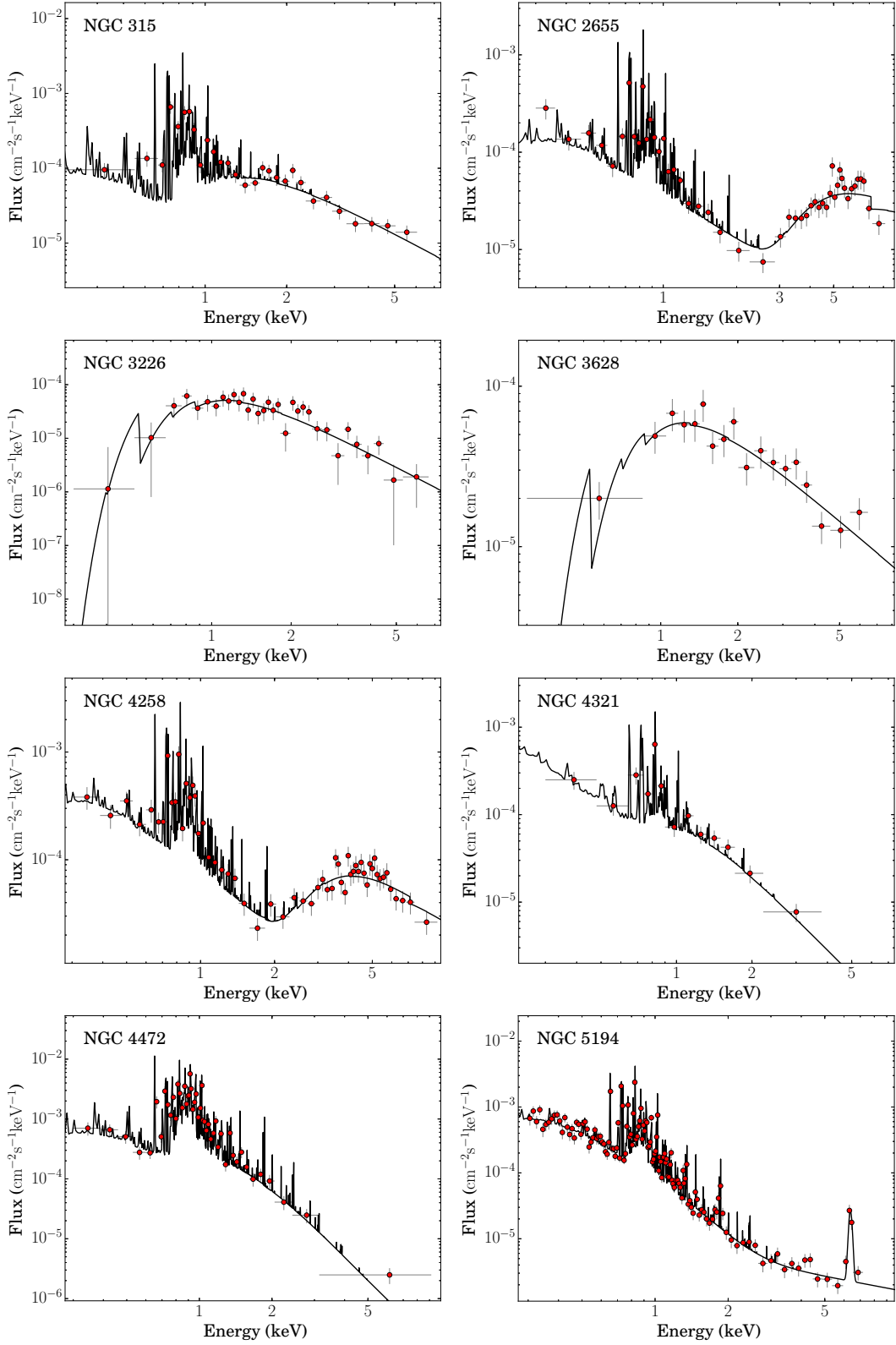


Figure A1. The middle flux-binned spectrum (unfolded) of each of the AGN in the sample for which flux-binning was carried out (excluding M81 - see Fig. 6). The best-fitting spectral model for each object is also shown in black.

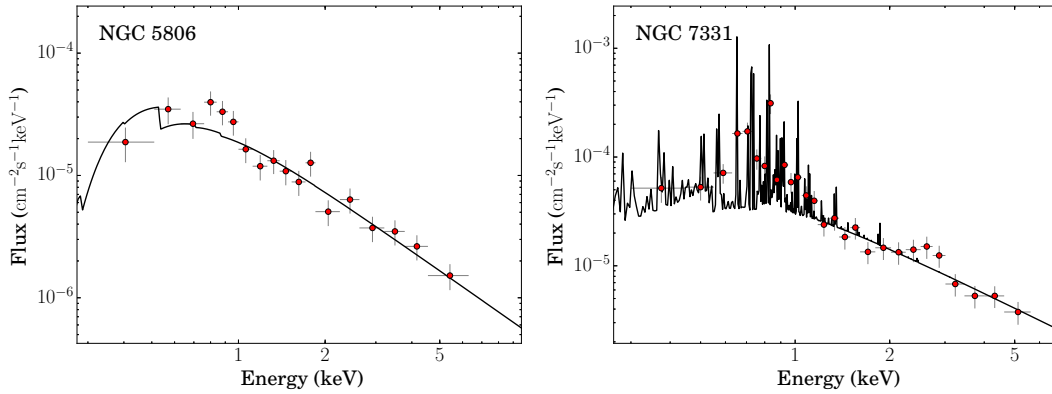


Figure A1. (Continued)

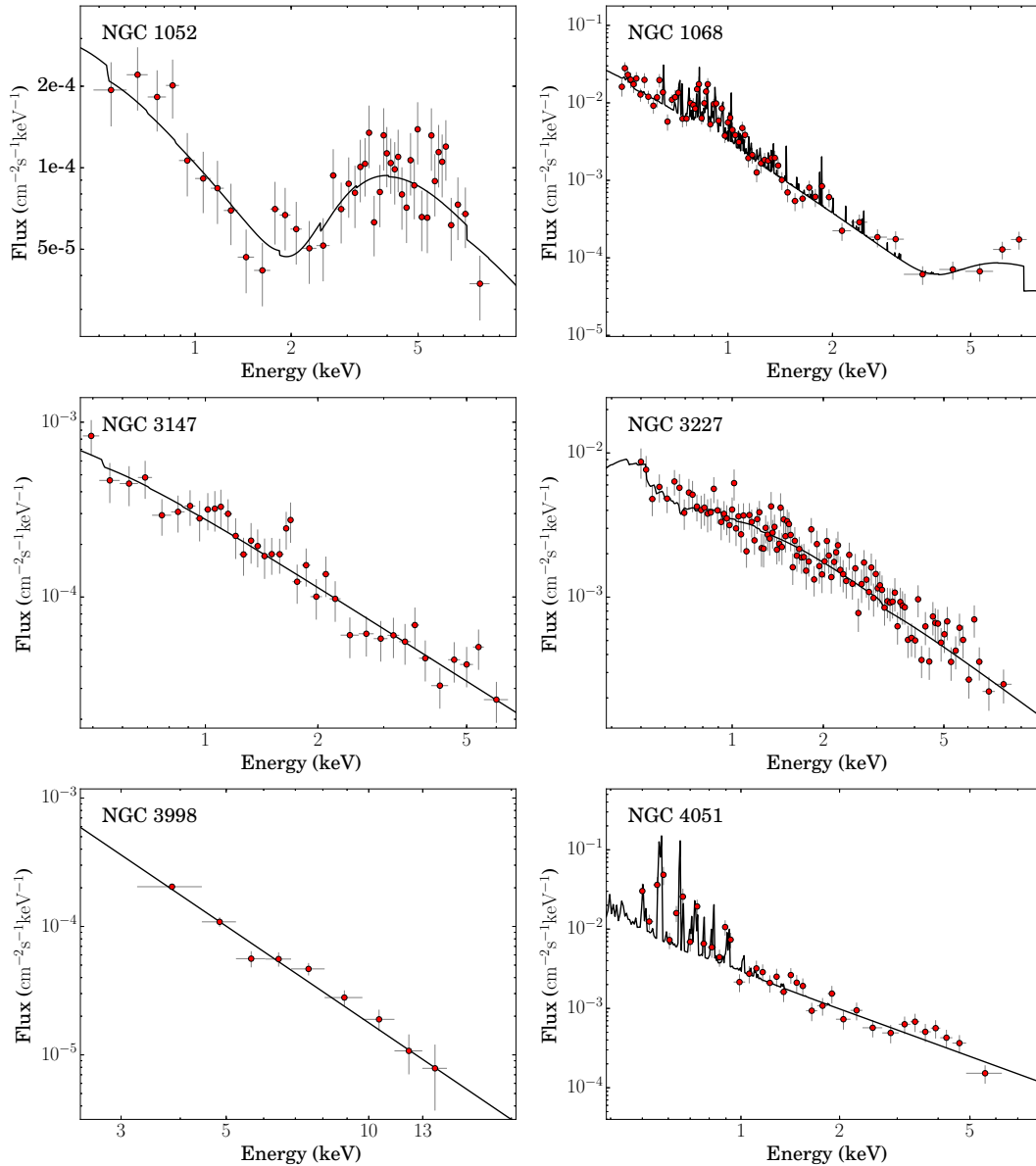


Figure A2. The total spectrum (unfolded) for each of the AGN in the sample for which flux-binning could not be carried out. The best-fitting spectral model for each object is also shown in black.

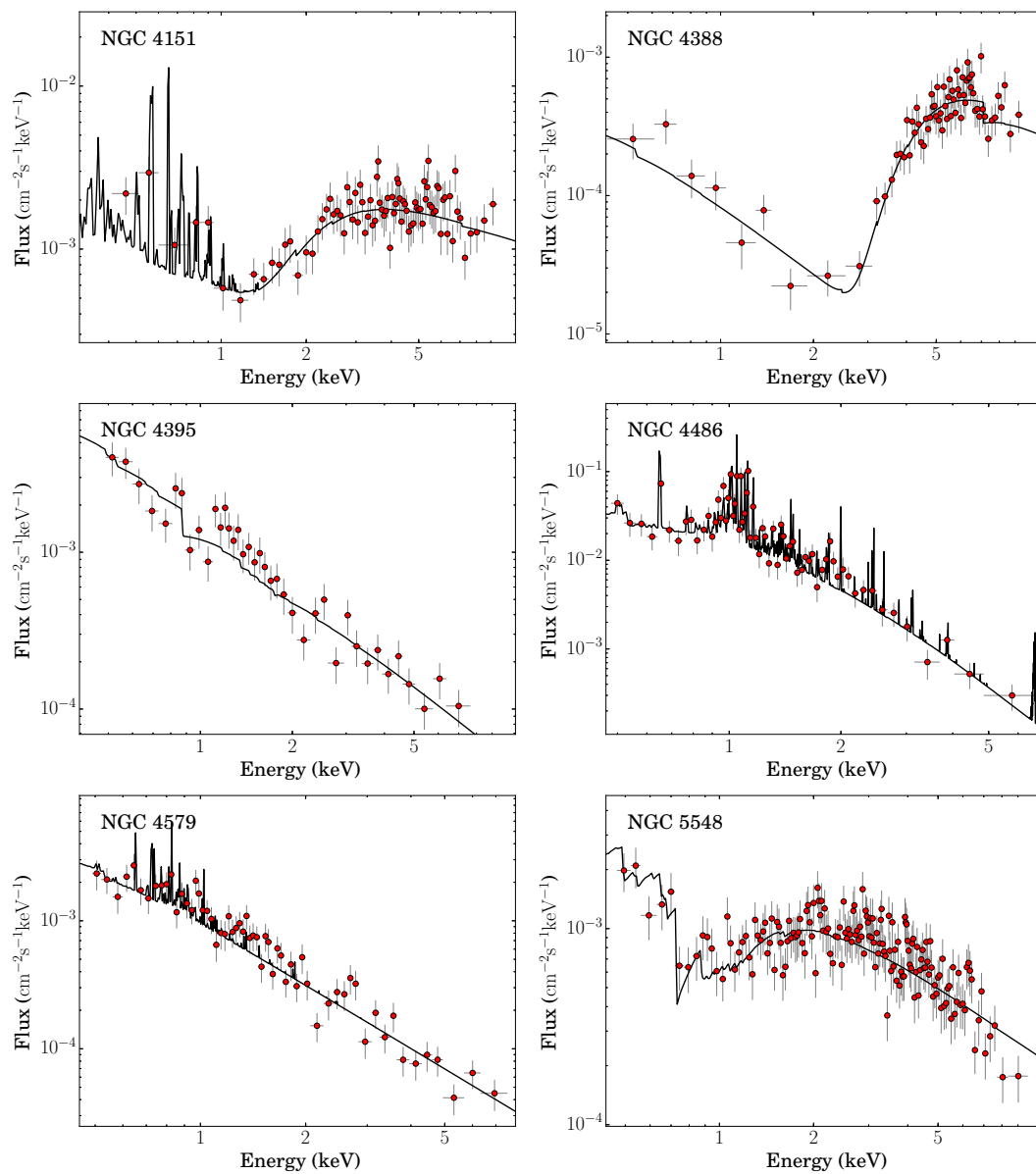


Figure A2. (Continued)